DYNAMIC RESPONSE AND WAVE PROPAGATION IN THREE-DIMENSIONAL FRAMED STRUCTURES

Y.-H. Pao *

Institute of Applied Mechanics
National Taiwan University
Taipei, Taiwan 10617, Taiwan

G.-H. Nie

Institute of Applied Mechanics
Tongji University
Shanghai 200092, China

D.-C. Keh

Development Engineer
Nassda Corporation
Taipei, Taiwan 10608, Taiwan

ABSTRACT

This paper extends the recently developed method of reverberation-ray matrix for planar structures to three-dimensional framed structures. The propagation of steady state axial, flexural and torsional waves, as well as the mode conversions through scattering of all three waves at connecting joints are evaluated in the frequency domain. The transient waves in all members are then determined by the Fourier synthesis. The transient responses of a two-storey framed building subject to a step time loading are calculated in detail. Numerical results are obtained for early time as well as moderately long time records. The results are shown to be accurate in arrival times of all three types of waves and in asymptotic values at times.

Keywords: 3D framed structures, Method of reverberation-ray matrix (MRRM), Dynamic response, Wave propagation.

1. INTRODUCTION

In this paper, we apply the recently developed method of reverberation-ray matrix (MRRM) [1-3] to analyze propagation of unidirectional elastic waves [4] and dynamic response of three-dimensional framed structures. The structure is made of a number of slender structural members connected at both ends by rigid or hinged joints with two or more other members in a pattern of three dimensional network, supported by fixed or moving foundations at a few base joints or floating in outer space. In MRRM, the integrand of inverse transform is expanded into a Neumann series expansion so as to remove singularities at natural frequencies of integration. Each integral of the expansion can thus be evaluated accurately by applying a Fast Fourier Transform (FFT) algorithm with minimal wraparound error. Numerical results as shown in this and previous papers demonstrate that we have achieved precise calculations of transient responses of a structure at early time hitherto unobtainable by other methods.

The dynamics of framed structures has been studied for more than a century, and applications of matrix analysis to mechanics of structures and continuous media began in 1930s [5]. Early in 1934-1935, Duncan and Collar formulated discrete flexibility matrix for solving problems of aeroelasticity in two papers [6,7], which are contained in a book co-authored with Frazer [8]. Several other matrix formulations were developed later, and that of unified forces and displacements was developed by Argyris and Kelsey [9]. In 1959, Turner reported direct stiffness matrix method in a comprehensive study [10] which encompassed structural and continuum models, as well as nonlinear, stability and dynamic simulations. It also presented efficient and general computer implementation, known later as the finite element method.

In the meantime, methods of matrix analysis of structures were been developed in fields of civil, mechanical, and other branches of engineering. In early 1950s, Myklestad [11] and Thomson (1950) formulated the method of transfer matrix (MTM) for analyzing vibration of a non-uniform beam, and for elastic waves in a vertically stratified media [12,13]. By mid-1960s, several methods of matrix analyses of static and steady state motion of structures and solids were essentially completed, as discussed in texts by Pestel and Leckie [14], Weaver and Gere [15], and Clough and Penzien [16] and others. It was understood at that time, transient response of a structure could be determined from

* Corresponding author (yhpao.iam.ntu@gmail.com)

DOI : 10.1017/jmech.2012.146
Copyright © 2013 The Society of Theoretical and Applied Mechanics, R.O.C.
https://doi.org/10.1017/jmech.2012.146 Published online by Cambridge University Press

inverse Laplace or Fourier transform of steady state response, or by an expansion in series of normal modes at all frequencies. Accurate numerical evaluation of the inverse transform integral, was, however, neither accurate nor efficient until Cooley and Tukey developed the first algorithm of Fast Fourier transform [17], and large electronic digital computers became available after 1965. Propagations of wave in structures were discussed later in a book by Doyle [18], which was revised in 1997 to include author's method of the latest research development. Additional recent research work is cited later in this paper.

The methods of reverberation-ray matrix analysis for two or three-dimensional motions of structures are quite different from all aforementioned methods. The major difference is the employing of two lengthwise coordinates for every structure member, each being originated from one of two end-joints, and the assuming of traveling wave solutions with unknown amplitude-coefficients and pre-assigned wave functions in dual coordinate for each mode of six waves in a member. The unknown coefficients are then determined from the boundary conditions (joint-coupling equations plus compatibility conditions of response) at the origin of each coordinate, without the use of transfer matrix to connect responses at two-end joints. In other words, we have reduced a two-point boundary value problem of wave equations in single coordinate to a pair of one-point boundary value problems in dual coordinates. Details of the differences and comparisons with traditional methods are discussed in two review articles by first author and colleagues [19,20] after the first draft of this paper was written. We have regrouped some of the details and inserted them as subsections with heading remarks at appropriate places of the revised manuscript. Finally, we note that the MRRM has also been formulated for propagation of elastic waves in layered media [21,22], like that of the transfer matrix [12,13], which will not be discussed here.

2. DYNAMIC EQUATIONS AND OF STRUCTURAL MEMBER AND TRAVELING WAVE SOLUTIONS

We consider motion and deformation of a three-dimensional framed structure which is composed of many slender rods connected at both ends by joints to form a pattern of network in space. The entire structure is in a state of static equilibrium initially, and is excited into motion by external forces and moments applied at joint, or by moving support. As in illustrative example, we show in Fig. 1(a), a two-storey framed building made of 16 structural members connected at 12 joints, with four base joints at foundation. There could be a few additional diagonal members for reinforcing lateral rigidity, which are omitted here. The frame could also be a part of aerospace structure floating in air or outer space if the four base joints are also connected by additional structural members. At the intersection of two or more members, each joint is considered a small rigid body capable of translating and rotating in space. Each structural member of length l is uniformed in cross sectional area A, and is made of elastic materials with constant mass density ρ, Young's modulus E, shear modulus G, and Poisson's ratio v, relating to E and G by $E/G = 2(1+v)$. Other geometric and material parameters of the structure will be defined when they arise.

2.1 Motion in Global and Local Coordinates Systems

Let the number of joints be n and that of structural members be m. For the structure shown, the joints are identified by numerals 1 to 12 or by letters J, K, L,…, and the structural members by two numerals or letters of both end joints (1–2, 2–3, …or JK, KL, …). We thus denote the number of members that connect to the common joint, say J by m^J, and $\sum_{J=1}^{n} m^J = 2m$.

The positions of all joints are referred to a fixed Cartesian coordinate O–X, Y, Z, named the global coordinate system. In the method of reverberation ray matrix, we introduce two right-handed Cartesian coordinate systems for any member JK, the ones originated from joint J being labeled as $(x, y, z)^{JK}$, and the other from joint K as $(x, y, z)^{KJ}$. They form dual local coordinate systems for each member, as shown in Fig. 1(b). The direction of the axis, passing through centroids of all cross sections, x^{JK} is always opposite to that of x^{KJ}, that of y^{KJ} is opposite to y^{JK} by choice, and thus the direction of z^{KJ} is the same as that of z^{JK}.

The entire structure is in static equilibrium at its initial (reference) configuration at time $t = t_0$ (initial time). Under combined action of applied forces and reactive forces from joints and supports, the structure moves to new position at current time $t(\geq t_0)$ in its current (deformed) configuration. Initially, all structural joints in equilibrium are at $\mathbf{X}(t_0) \equiv \mathbf{X}_0$. As time increases, they are moved to current positions $\mathbf{X}(t)$ in translational motion $\mathbf{U}(t) = \mathbf{X}(t) - \mathbf{X}_0$ and rigid rotation $\mathbf{\Phi}(t)$.

The motion of each structural member is, however, much more complicated because it moves with the joints as well as deforms in between end joints. In one dimensional theory of elastodynamics, one considers first the motion of a differential mass element $\rho(x)A(x)dx$ of differential length along x-axis passing through centroids of all cross sectional area $A(x)$. The local axes y and z are oriented along two principle axes of the plane area $A(x)$. The mass element is bounded by lateral surface of the member and two rigid cross sectional planes $A(x)$ and $A(x + dx)$ (along x-axis). Initially, the two planes are at reference positions $x(t_0) \equiv x_0$ and $x_0 + dx_0$ respectively along the x–$axis$. At time t, the plane $A(x)$ is moved rigidly to current position at $\mathbf{x}(t)$ with displacement $\mathbf{u}(t) = \mathbf{x}(t) - \mathbf{x}_0$ and additional rigid rotation $\boldsymbol{\varphi}(t)$ about three local axes, the three components of $\mathbf{u}$ being $u_x = x(t) - x_0$, $u_y = y(t)$, and $u_z = z(t)$, and those of $\boldsymbol{\varphi}(t)$ being ϕ_x, ϕ_y, ϕ_z. At the same time, the cross sectional plane $A(x + dx)$ is moved to current position $\mathbf{x}(t) + d\mathbf{x}$ with displacement $\mathbf{u}(t) + d\mathbf{u}$

https://doi.org/10.1017/jmech.2012.146 Published online by Cambridge University Press

and rotation $\boldsymbol{\varphi}(t) + d\boldsymbol{\varphi}$. The mass element is thus bent and twisted, and the differential length between two bounding planes is increased by the amount $dx - dx_0 = du_x$.

The deformed mass element is subjected to actions from both sides of the elastic structural member. From the left-hand side ($-x$ direction), the action is represented by tractions $t^{(-x)}$ (distributive force per unit area) over area-element dA of $A(x)$, giving rise to internal surface-force vector $\mathbf{F}(x)$ plus internal moment vector $\mathbf{M}(x)$, as defined by following surface integrals,

$$\mathbf{F} = \int_A \mathbf{t}^{(-x)} dA; \mathbf{M} = \int_A \mathbf{r} \times \mathbf{t}^{(-x)} dA \tag{1}$$

where the moment arm r is directed from centroid to dA of the same plane. Similarly, the resultant action from the right-hand side ($+x$ direction) of cross section $A(x + dx)$ is represented by $\mathbf{F}(x) + d\mathbf{F}$ and $\mathbf{M}(x) + d\mathbf{M}$.

We shall denote Cartesian components of all physical vectors in global coordinates by majuscule Latin subscripts like U_I^{JK}, $I = X, Y, Z$, and those in local coordinates by minuscule Latin subscripts u_i^{JK}, $i = x, y, z$. The three Cartesian components of the tractions are also components of a stress tensor $\boldsymbol{\sigma}(\mathbf{x})$, acting on the plane normal to $\pm x$–axis, $t_i^{(\pm x)} \equiv \sigma_{xi}$, $i = x, y, z$. For this reason, F_i and M_i are also called stress resultant and stress-moment resultant respectively. The components of vector $\mathbf{u}$ or $\mathbf{F}$ (and $\boldsymbol{\varphi}$ or $\mathbf{M}$) may also be converted to those in global coordinates by the transformation matrix $\mathbf{T}$ as follows,

$$U_J = \sum_i T_{Ji} u_i \ , \ (i = x, y, z; J = X, Y, Z) \tag{2}$$

where $T_{Ji} = \cos \theta_{Ji}$, and θ_{Ji} is the angle subtended by x_i and X_J. The sign convention of point vector $\mathbf{u}$ or $\boldsymbol{\varphi}$ follows that of base-vectors along three coordinate axes. As for the surface-point vectors $\mathbf{F}$ and $\mathbf{M}$, the sign convention follows that of stress tensors, and a component is positive if it acts on a positive (negative) plane along positive (negative) local axis. Otherwise, it is negative. All surface-forces and moments shown in Fig. 1(b) are positive.

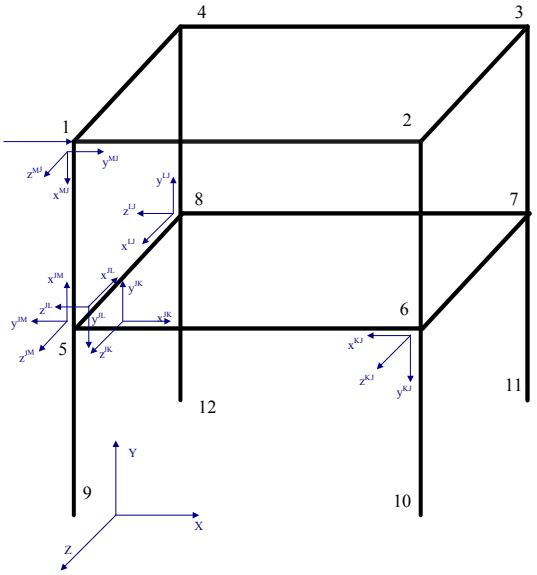
For all vector components in dual local coordinate system, there is additional complication in sign conventions because the directions of x^{JK} and x^{KJ} are reversed but those of z^{JK} and z^{KJ} are not. At the same cross sectional area designated by x^{JK} or $x^{KJ} = l - x^{JK}$, the components of two displacement vectors $\mathbf{u}^{JK}$ and $\mathbf{u}^{KJ}$ (or $\boldsymbol{\varphi}^{JK}$ and $\boldsymbol{\varphi}^{KJ}$) at the same point are related by the following sign convention,

$$(u_x, u_y, u_z)^{JK} = (-u_x, -u_y, u_z)^{KJ} \tag{3a}$$

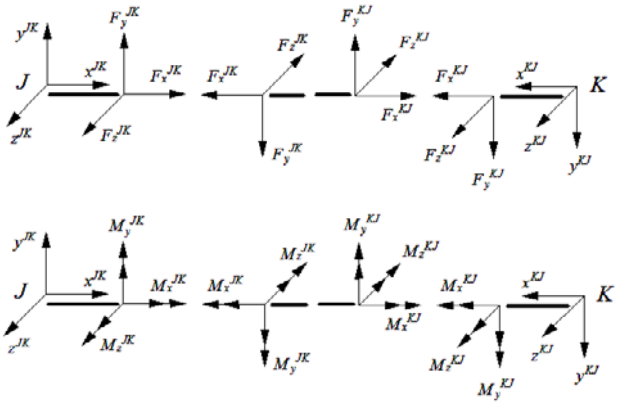
The components of $\mathbf{F}^{JK}$ and $\mathbf{F}^{KJ}$ (or $\mathbf{M}^{JK}$ and $\mathbf{M}^{KJ}$) at same cross sections are related by different sign conventions as follows,

$$(F_x, F_y, F_z)^{JK} = (F_x, F_y, -F_z)^{KJ} \tag{3b}$$

This rather complicated sign convention must be rigidly adhered in analyses and calculations.



(a) Frame joint, member index and coordinate systems



(b) Sign convention for internal forces and moments

Fig. 1 Geometry of a framed structure and sign convention for internal forces and moments

2.2 Equations of Motion for Transient and Steady-state Waves

In one dimensional theory of elastodynamics, the motion of a one dimensional mass element $\rho A dx$ of lengthwise dx along x-axis of each member is expressed in terms of displacement vectors $\mathbf{u}(u_x, u_y, u_z)$ of cross sectional plane area $A(x)$ and rigid rotation vector of the plane $\boldsymbol{\varphi}(\phi_x, \phi_y, \phi_z)$ about three principal axes (x–, y–, z–) of the area. The dominant motion of the mass element with six degrees of freedom is represented by four types of wave motion, governed by four sets of second order of partial differential equations. The first two sets are standard wave equations with different speeds, governing longitudinal motion u_x of the plane area in lengthwise direction, and torsional motion ϕ_x of the plane, rotating about x- axis respectively. The third set governs flexural motion of the mass element in x-y plane, consisting of two second order equations coupling transverse displacement u_y and rotation ϕ_z about transverse the z- axis. The forth set governs flexural motion in x-z plane, consisting of two equations coupling transverse displacement u_z and rotation of the plane ϕ_y about transverse the y- axis.

https://doi.org/10.1017/jmech.2012.146 Published online by Cambridge University Press

The partial differential equations for $u_i(x,t)$ and $\phi_i(x,t),(i = x, y, z)$ may be reduced to four ordinary differential equations for sets of $\bar{u}_i(x, \omega)$ and $\bar{\phi}_i(x, \omega)$, called steady state or reduced equation of motion, by applying Fourier transform or simply separating variables and assuming $\mathbf{u}(x, t) = \bar{\mathbf{u}}(x, \omega)\, e^{i\omega t}$ and $\phi(x, t) = \bar{\phi}(x, \omega)\, e^{i\omega t}$. The pair of Fourier integrals, defining Fourier transform of $\mathbf{u}(x, t)$ and inverse Fourier transform $\bar{\mathbf{u}}(x, \omega)$ is listed below,

$$\bar{\mathbf{u}}(x, \omega) = \int_{-\infty}^{\infty} \mathbf{u}(x, t)\, e^{-i\omega t}\, dt\,;$$
$$\bar{\mathbf{u}}(x, \omega) = \mathcal{F}\{\mathbf{u}(x, t)\}: \tag{4a}$$

$$\mathbf{u}(x, t) = \frac{1}{2\pi}\int_{-\infty}^{\infty} \bar{\mathbf{u}}(x, \omega)\, e^{i\omega t}\, d\omega\,;$$
$$\mathbf{u}(x, t) = \mathcal{F}^{-1}\{\bar{\mathbf{u}}(x, \omega)\}: \tag{4b}$$

The pair of integral transforms may be expressed symbolically by introducing Fourier transform operator $\mathcal{F}$ and inverse Fourier transform operator $\mathcal{F}^{-1}$ as shown in previous equations.

In this paper we consider that all external force and action are applied at joints of a structure in the form of concentrated dynamic force $\mathbf{f}^J(t)$ and point-couple $\boldsymbol{\mu}^J(t)$, or prescribed motion imposed on the joint. In case a concentrated force is applied at intermediate point of a member, we insert an artificial joint under the force and split the member fictitiously into two. The response of the structure in the form of joint displacement, $\mathbf{U}^J(t)$, member displacement $\mathbf{u}^{JK}(x, t)$, and internal force $\mathbf{F}^{JK}(x,t)$, and so on, are called transient wave- motion or transient responses of the structure. On the other hand, if the applied force is oscillating at single frequency ω (simple harmonic excitation), $\mathbf{f}^J(t) = \bar{\mathbf{f}}^J(\omega)\, e^{i\omega t}$, $(-\infty < t < \infty)$ the displacement- or velocity-response is also harmonic in time, $\mathbf{u}(x, t)$ by $\bar{\mathbf{u}}(x, \omega)e^{i\omega t}$, they are known as steady state wave- motion.

We list below four sets of ordinary differential equations governing four types of steady state motion in six modes of wave propagation in structural members without further discussions.

1. Axial Wave Motion

Along the x-axis of the mass element $\rho A dx$, the axial wave motion is governed by equation of linear momentum for net axial force $\partial F_x / \partial x(dx)$, coupled with axial strain by constitutive equation (Hooke's Law) in the following

$$\frac{\partial F_x}{\partial x} = \rho A \frac{\partial^2 u_x}{\partial t^2}\ ;\ F_x(x, t) = EA\frac{\partial u_x}{\partial x} \tag{5}$$

The previous two equations may be combined to form standard wave equations for homogeneous and uniform structural members,

$$\frac{\partial^2 u_x}{\partial x^2} = \frac{1}{c_0^2}\frac{\partial^2 u_x}{\partial t^2},\ c_0^2 = \frac{E}{\rho} \tag{6a}$$

where c_0 is the constant speed of longitudinal wave in a rod. The reduced wave equation for steady state motion is,

$$\frac{d^2\bar{u}_x}{dx^2} = -\left(\frac{\omega}{c_0}\right)^2 \bar{u}_x \tag{6b}$$

2. Torsional Wave Motion

Similarly for torsional motion of a circular or nearly circular rod, the angular momentum equation and constitutive equation for the angle of twist ϕ_x and torsional moment M_x are

$$\frac{\partial M_x}{\partial x} = \rho I_x \frac{\partial^2 \phi_x}{\partial t^2}\ ;\ M_x = GI_x\frac{\partial \phi_x}{\partial x} \tag{7}$$

where $I_x = A\gamma_x^2$ is the second moment of area A about the x–axis, and γ_x the corresponding radius of gyration. Again, they are combined to form the wave equation for ϕ_x with shear wave speed c_s, and reduced wave equation for $\bar{\phi}_x(x, \omega)$ as follows

$$\frac{\partial^2 \phi_x}{\partial x^2} = \frac{1}{c_s^2}\frac{\partial^2 \phi_x}{\partial t^2},\ c_s^2 = \frac{G}{\rho} \tag{8a}$$

$$\frac{d^2\bar{\phi}_x}{dx^2} = -\left(\frac{\omega}{c_s}\right)^2 \bar{\phi}_x \tag{8b}$$

3. Flexural Wave Motion in *x–y* Plane

The theory of flexural motion of a structural member was developed by Bernoulli and Euler around 1755 and modified by Rayleigh and Timoshenko [23] to include effects of rotatory inertia and shear deformation. Linear momentum equations for u_y and angular momentum equation for ϕ_z of the mass element $\rho A dx$ are given respectively by,

$$\frac{\partial F_y}{\partial x} = \rho A\frac{\partial^2 u_y}{\partial t^2}\ ;\ \frac{\partial M_z}{\partial x} + F_y = \rho I_z\frac{\partial^2 \phi_z}{\partial t^2} \tag{9a}$$

where I_z (or I_y) is another second moment area about the principle axis the z (or y) and $I_j = A\gamma_j^2 (j = x, y, z)$, the three principle radii of gyration γ_j being related by $\gamma_x^2 = \gamma_y^2 + \gamma_z^2$. The constitutive equation for shear force F_y and that for bending moment M_z are

$$F_y = \kappa AG\left(\frac{\partial u_y}{\partial x} - \phi_z\right);\ M_z = EI_z\frac{\partial \phi_z}{\partial x} \tag{9b}$$

In the first equation, the shear factor κ is assumed to vary with cross sectional area A by Timoshenko [23], and to have constant value of $\pi^2/12$ by Mindlin [24]. Elimination of M_z and F_y from these four equations gives rise to the following coupled differential equations of flexural wave, (u_y, ϕ_z), in the principal x-y plane of a beam

$$\frac{\partial^2 u_y}{\partial x^2} - \frac{\partial \phi_z}{\partial x} = \frac{1}{\kappa c_s^2}\frac{\partial^2 u_y}{\partial t^2}, \tag{10a}$$

$$\frac{\partial^2 \phi_z}{\partial x^2} + \frac{\kappa c_s^2}{\gamma_z^2 c_0^2}\left(\frac{\partial u_y}{\partial x} - \phi_z\right) = \frac{1}{c_0^2}\frac{\partial^2 \phi_z}{\partial t^2} \tag{10b}$$

https://doi.org/10.1017/jmech.2012.146 Published online by Cambridge University Press

where the c_s is the shear wave speed defined previously. The reduced equations of steady state flexural wave motion may simply be deduced from previous ones by replacing $u(x, t)$ and $\phi(x, t)$ by $\bar{\phi}(x, \omega)$ and $\bar{\phi}(x, \omega)$, and by replacing the operator $\partial/\partial t$ with $(i\omega)$, and $\partial^2/\partial t^2$ by $(-\omega^2)$.

The previous two motion Eqs. (10a,10b) may be combined further to form a single fourth-order equation for u_y, known as the Timoshenko beam equation as follows

$$EI_z \frac{\partial^4 u_y}{\partial x^4} - \rho I_z \left(1 + \frac{AE}{\kappa AG}\right) \frac{\partial^4 u_y}{\partial x^2 \partial t^2} + \frac{\rho I_z \rho A}{\kappa AG} \frac{\partial^4 u_y}{\partial t^4} + \rho A \frac{\partial^2 u_y}{\partial t^2} = 0$$

It is simplified to classical Euler-Bernoulli beam equation if the effects of rotatory inertia and shear are neglected by setting $\rho I_z \to 0$ and $\kappa AG \to \infty$.

4. **Flexural Wave Motion in *x–z* Plane**

A similar set of equations is deduced for the transverse displacement u_z and rotation ϕ_y about y-axis for each member in the second principal plane x-z along the beam

$$\frac{\partial F_z}{\partial x} = \rho A \frac{\partial^2 u_z}{\partial t^2}\ ;\ \frac{\partial M_y}{\partial x} + F_z = \rho I_y \frac{\partial^2 \phi_y}{\partial t^2} \tag{11a}$$

The corresponding constitutive equations for shear force F_z and bending moment M_y are

$$F_z = \kappa AG\left(\frac{\partial u_z}{\partial x} - \phi_y\right);\ M_y = EI_y \frac{\partial \phi_y}{\partial x} \tag{11b}$$

Again, these four equations maybe combined to form two second order differential equations for u_z and ϕ_y

$$\frac{\partial^2 u_z}{\partial x^2} - \frac{\partial \phi_y}{\partial x} = \frac{1}{\kappa c_s^2} \frac{\partial^2 u_z}{\partial t^2}, \tag{12a}$$

$$\frac{\partial^2 \phi_y}{\partial x^2} + \frac{\kappa c_s^2}{\gamma_y^2 c_0^2}\left(\frac{\partial u_z}{\partial x} - \phi_y\right) = \frac{1}{c_0^2} \frac{\partial^2 \phi_y}{\partial t^2} \tag{12b}$$

The reduced equation of motion for steady state flexural wave in x-z may be deduced accordingly.

The four sets of six differential equations, Eqs. (6a), (8a), (10a) and (10b), and (12a) and (12b) formulate complete set of dynamic equations for a structural member in either one of dual coordinates x^{JK} and x^{KJ} and arbitrary time t. Dynamic equations for steady state wave motion can simply be deduced by replacing time derivative operator with exponents by separating spatial part from the temporal part of simple harmonic motion at single frequency.

2.3 Steady State Wave Motion

Solutions for steady state wave equations in Eqs. (6a), (8a), (10a,b) and (12a,b) can all be obtained from linear combination of traveling plane harmonic waves of the form $Be^{i(\pm kx + \omega t)}$, where B is an arbitrary constant representing wave amplitude, and in the phase function, ratio of the wave number k to frequency ω equals by definition phase velocity $c = \mp\omega/k$ of the plane harmonic wave. Two of the three wave parameters k, ω, c must satisfy the characteristic equation of Eqs. (6), (8), (10) or (12) which admits the plane wave functions as a solution.

We list below, plane wave solutions for six modes of traveling wave with different wave numbers k_α and unknown amplitude coefficients a_α and $d_\alpha(\alpha = 1, 2, \ldots, 6)$, the time factor $e^{i\omega t}$ common to all waves in each and every structural member as well as joints being omitted.

1. **Axial Waves**

$$\bar{u}_x(x, \omega) = a_1(\omega)e^{ik_1 x} + d_1(\omega)e^{-ik_1 x}\ ;\ k_1 = \omega/c_0 \tag{13}$$

2. **Torsional Waves**

$$\bar{\phi}_x(x, \omega) = a_2(\omega)e^{ik_2 x} + d_2(\omega)e^{-ik_2 x}\ ;\ k_2 = \omega/c_s \tag{14}$$

3. **Flexural Waves in *x–y* Plane**

$$\bar{u}_y(x, \omega) = a_3(\omega)e^{ik_3 x} + d_3(\omega)e^{-ik_3 x} + a_4(\omega)e^{ik_4 x} + d_4(\omega)e^{-ik_4 x} \tag{15a}$$

$$\bar{\phi}_z(x, \omega) = \alpha_3\, a_3(\omega)e^{ik_3 x} - \alpha_3\, d_3(\omega)e^{-ik_3 x} + \alpha_4\, a_4(\omega)e^{ik_4 x} - \alpha_4\, d_4(\omega)e^{-ik_4 x} \tag{15b}$$

4. **Flexural Waves in *x–z* Plane**

$$\bar{u}_z(x, \omega) = a_5(\omega)e^{ik_5 x} + d_5(\omega)e^{-ik_5 x} + a_6(\omega)e^{ik_6 x} + d_6(\omega)e^{-ik_6 x} \tag{16a}$$

$$\bar{\phi}_y(x, \omega) = \alpha_5\, a_5(\omega)e^{ik_5 x} - \alpha_5\, d_5(\omega)e^{-ik_5 x} + \alpha_6\, a_6(\omega)e^{ik_6 x} - \alpha_6\, d_6(\omega)e^{-ik_6 x} \tag{16b}$$

In previous solutions, the unknown frequency dependent amplitudes $a_\alpha(\omega)$ and $d_\alpha(\omega)$ are designated as the arriving and departing wave amplitudes respectively, four waves propagating towards and away from the end joint ($x = 0$) which originates one of dual coordinates in each member. The wave number k_α and amplitude ratio $\alpha_{3,4}$ are determined form respective characteristic equations as follows:

$$\left(\frac{c_0\, k_{3,4}}{\omega}\right)^2 = \frac{1}{2}\left(1 + \frac{E}{\kappa G}\right) \pm \frac{1}{2}\sqrt{\left(1 + \frac{E}{\kappa G}\right)^2 - 4\left(\frac{E}{\kappa G} - \frac{c_0^2}{\gamma_z^2 \omega^2}\right)} \tag{17a}$$

The amplitudes ratios $\alpha_{3,4}$ are given by

$$\alpha_{3,4} = \frac{1}{ik_{3,4}}\left(\frac{\omega^2}{\kappa c_s^2} - k_{3,4}^2\right), \tag{17b}$$

We summarize all typical numerical results by the dispersion spectra in wave number as illustrated by Fig. 2 (using AISC MC18 × 58 as example and $l_0 = 0.9144$m, $E = 70.0$GPa, $\nu = 0.3$, $\rho = 2700.0$kg/m^3 as described in

https://doi.org/10.1017/jmech.2012.146 Published online by Cambridge University Press

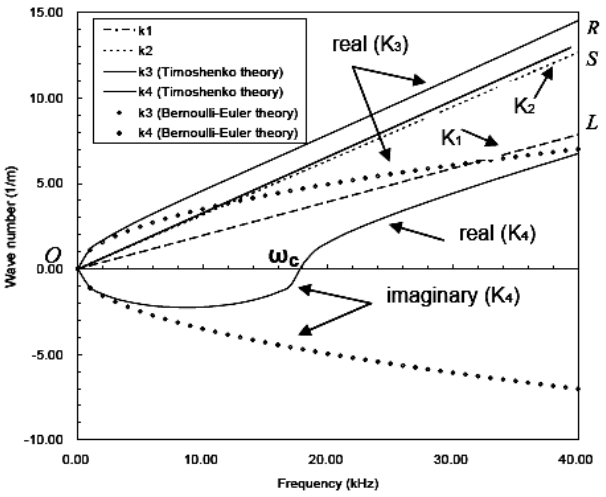


Fig. 2 Dispersion spectra in wave numbers

section 5), which is a plot of the real part of frequency (Reω) versus the real part of wave number (±Rek) and imaginary part of wave number (±Imk). The three wave parameters, circular frequency ω, the real part of wave number (Rek), and wave speed c, are related by the equation $c = \omega/k$. There are six branches of dispersion curves, one for each mode, but only four branches are shown in the figure. The branches for axial wave and torsional wave are shown as two straight lines respectively, OL with slope $1/c_0$ and OS with slope $1/c_s$. The branch for bending mode of flexural wave, k_3, starts from the origin O as a parabola, and approaching asymptotically the line OR with slope $1/c_r$ where c_r is the Rayleigh surface wave velocity in a half space. The branch for single shear mode of flexural wave, k_4, starts at the cut off frequency ω_c as a hyperbola, approaching a straight line with slope $1/(\sqrt{\kappa}\, c_s)$ in real wave number plane. Below ω_c, it bends toward the origin in either positive or negative imaginary wave plane. Dispersion curves for the flexural waves in another plane, k_5 and k_6, are omitted here. Each point on a branch represent a mode of wave propagation with frequency ω, wave number k, and phase velocity $c_\alpha(\alpha = 1, 2, \ldots, 4)$, which equals the ratio of abscissa ω to ordinate on the figure. The slope of tangent to the curve at the point equals inverse group velocity of the mode, $1/c_g$.

In Fig. 2, we show also dispersion spectra of four modes of flexural waves based upon classical Bernoulli-Euler theory, for which $(\omega/\gamma_z c_0)^{1/2} = \pm k$, $\mp(ik)$. They are shown as two parabolas in Rek and Imk planes in dotted lines, which coincide with dispersion curves of Timoshenko- Rayleigh theory only in a small neighborhood of origin. The comparison indicates clearly that the classical beam theory cannot be applied to analyze vibration of structure members at high frequencies.

2.4 Summary of Equations of Motions and Solutions in Matrix Form

For convenience of ensuing discussions, we summarize the equations of motion in section 2.2 and six modes of steady state traveling wave solutions in section 2.3 in the form of matrix. The two displacement vectors $\bar{\mathbf{u}}(x, \omega)$ and $\bar{\boldsymbol{\varphi}}(x, \omega)$ with components $\bar{u}_i$ and $\bar{\phi}_i (i = x, y, z)$ are physical vectors expressed in three dimensional Euclidian geometric space of (r^3) spanned by three unit base vectors along Cartesian coordinates x, y, z. They are grouped to form the dynamic displacement-state vector $\bar{\mathbf{u}}^s(\bar{u}_i, \bar{\phi}_i)$ in a six dimensional vector space, expressed by a column matrix of six elements, $\bar{u}^s_\alpha(\bar{u}_x, \bar{\phi}_x, \bar{u}_y, \bar{\phi}_z, \bar{u}_z, \bar{\phi}_y)^t$, where the superscript t denotes transpose of the row matrix. The internal force vector $\bar{\mathbf{F}}(\bar{F}_i)$ and internal moment $\bar{\mathbf{M}}(\bar{M}_i)$ in Cartesian space are derived by substituting components of $\partial\bar{u}_i/\partial x$ or $\partial\bar{\phi}_i/\partial x$ into respective constitutive equations in Eqs. (5), (7), (9b) and (11b). They are similarly grouped to form dynamic force-state vector $\bar{\mathbf{F}}^s(x, \omega)$, expressed by a column matrix of six elements $\bar{F}^s_\alpha(\bar{F}_x, \bar{M}_x, \bar{F}_y, \bar{M}_z, \bar{F}_z, \bar{M}_y)^t$.

The six steady state equations of motion for each structural member, say J-K in Eqs. (6), (8), (10) and (12) may be summarized in one matrix equation of displacement-state vector $\bar{\mathbf{u}}^s(x, \omega)$,

$$\left[\boldsymbol{\mathcal{L}} + \omega^2 \boldsymbol{\mathcal{M}}(x, \omega)\right]\bar{\mathbf{u}}^s(x, \omega) = 0\,, \quad \text{(member } JK\text{)} \tag{18}$$

In the previous equation, $\boldsymbol{\mathcal{L}}$ is a 6 × 6 square matrix composed of three blocks of 2 × 2 sub-matrices consisting linear differential operators of d/dx and d^2/dx^2 along main diagonal; $\boldsymbol{\mathcal{M}}$ is another 6 × 6 square matrix with elements in material parameters as listed in Appendix. All square matrices and the displacement state vector $\bar{\mathbf{u}}^s$ as well as their components should be identified with superscript JK or KJ, which are omitted here in accordance with the dual coordinate x^{JK} and x^{KJ} for each member. The six steady state traveling wave solutions in Eqs. (13) ~ (16) are expressed in one matrix equation

$$\bar{\mathbf{u}}^s(x, \omega) = \mathbf{C}^u_+ \mathbf{P}(+\mathbf{k}x)\mathbf{a}(\omega) + \mathbf{C}^u_- \mathbf{P}(-\mathbf{k}x)\mathbf{d}(\omega)\,, \quad \text{(member } JK\text{)} \tag{19}$$

where the coefficient matrix in displacement $\mathbf{C}^u_\pm$ are two 6 × 6 square matrices, and the phase-function matrices $\mathbf{P}(\pm\mathbf{k}x)$ are two diagonal square matrices of six non-vanishing elements $e^{\pm ik\alpha x}(\alpha = 1, 2, \ldots, 6)$, as listed in Appendix. The six unknown amplitude coefficients a_α and $d_\alpha(\alpha = 1, 2, \ldots, 6)$ are expressed in column matrix $\mathbf{a}$ and $\mathbf{d}$ respectively.

Similarly, the dynamic force state vector $\bar{\mathbf{F}}^s(x, \omega)$ composed of six components $\bar{F}_i$ and $\bar{M}_i$ is expressed by the following matrix equation,

$$\bar{\mathbf{F}}^s(x, \omega) = \mathbf{C}^f_+ \mathbf{P}(+\mathbf{k}x)\mathbf{a}(\omega) + \mathbf{C}^f_- \mathbf{P}(-\mathbf{k}x)\mathbf{d}(\omega)\,; \quad \text{(member } JK\text{)} \tag{20}$$

https://doi.org/10.1017/jmech.2012.146 Published online by Cambridge University Press

Only the 6 × 6 coefficient matrices in force $\mathbf{C}_{\pm}^{f}$ differ from the corresponding coefficient in displacement as shown in Appendix. The other matrices in Eq. (20) are the same as those in Eq. (19).

3. BOUNDARY CONDITIONS AND REVERBERATION-RAY MATRIX

In the steady state traveling wave solutions expressed by Eqs. (19) and (20), the unknown wave-amplitude vector $\mathbf{a}(a_\alpha)$ and $\mathbf{d}(d_\alpha)$, (α = 1, 2, …, 6) for each structural member are usually determined from prescribed kinematic or kinetic boundary conditions at both end joints. Since each end joint of a structure is also in motion, the usual boundary conditions are then replaced by a set of joint coupling equations consisting of dynamic equations of a moving joint and continuity conditions of displacements at each joint. In addition, there is another set of compatibility conditions of displacements in each member, which is specially developed in MRRM as discussed in this section.

We assumed all external forces and moments are applied at joints of a structure, and denote concentrated force at the joint J by $\mathbf{f}^J(t) = \bar{\mathbf{f}}(\omega)\, e^{i\omega t}$ and concentrated moments by $\boldsymbol{\mu}^J(t) = \bar{\boldsymbol{\mu}}(\omega)\, e^{i\omega t}$, where $\bar{\mathbf{f}}(\omega)$ and $\bar{\boldsymbol{\mu}}(\omega)$ are Fourier transforms of respective force and moment. A concentrated force (or moment) applied at the middle of a member is treated as a joint force (or moment) by inserting artificially an extra joint under the force. The steady state response of each member expressed by matrix Eqs. (19) and (20) is thus excited by external sources of harmonic time function applied at bonding joints. The responses are evaluated in the following subsections.

3.1 Joint Coupling Equations

Let a typical joint J of a structure be connected to m^J-number of structural members, $J\Lambda(\Lambda = 1, 2, \ldots, m^J)$ with dual coordinate $x^{J\Lambda}$ and $x^{\Lambda J}$. For example, around the joint J (No.5) in Fig. 1(a), $m^J = 4$ and Λ = 1, 6, 8, 9 or I, K, L, and M. Under combined actions of external force $\mathbf{f}^J(t)$ and internal force-vectors $\mathbf{F}^{J\Lambda}(x, t)$ and moment-vectors $\mathbf{M}^{J\Lambda}(x, t)$, motion of the joint J with point mass M^J and principle moment of inertia tensor $\mathbf{I}^J$ is governed by following balance equations of linear momentum, and of angular momentum ($M^J\dot{\mathbf{U}}^J(t)$ and $\mathbf{I}^J\cdot\dot{\boldsymbol{\Phi}}^J(t)$) for steady state responses,

$$\sum_{\Lambda=1}^{m^J}\sum_{i=1}^{3}(T_{Ki}^{J\Lambda})^{-1}\bar{F}_i^{J\Lambda}(0,\ \omega)+\bar{f}_K^J=-\omega^2 M^J\bar{U}_K^J(\omega) \quad (21a)$$

$$\sum_{\Lambda=1}^{m^J}\sum_{i=1}^{3}(T_{Ki}^{J\Lambda})^{-1}\bar{M}_i^{J\Lambda}(0,\ \omega)+\bar{\mu}_K^J=-\omega^2 I_K^J\bar{\Phi}_K^J(\omega) \quad (21b)$$

In the previous vector equations in global component of subscript K ($K = X, Y, Z$), all internal force vectors and moment vectors are evaluated at $x^{J\Lambda} = 0$ in local coordinates of each member. The components in local coordinates have been transformed to those in global coordinates by applying Eq. (2) and then summed over all members around the joint J.

Furthermore, if all members are rigidly connected to the common joint, the displacement and rotation of each member at $x^{J\Lambda} = 0$ should be continuous with those of joints, $\bar{U}_K^J$ and $\bar{\Phi}_K^J$. The conditions of continuity of displacements and rotations for each and every connecting member give rise to a set of m^J number vector equations for $\bar{\mathbf{u}}^{J\Lambda}(0, \omega)$ and another set for $\bar{\boldsymbol{\varphi}}^{J\Lambda}(0, \omega)$,

$$\sum_{i=1}^{3}(T_{Ki}^{J\Lambda})^{-1}\bar{u}_i^{J\Lambda}(0,\ \omega)=\bar{U}_K^J\ ,\ \Lambda=1,\ 2,\ 3,\ \ldots,\ m^J \quad (22a)$$

$$\sum_{i=1}^{3}(T_{Ki}^{J\Lambda})^{-1}\bar{\phi}_i^{J\Lambda}(0,\ \omega)=\bar{\Phi}_K^J\ ,\ \Lambda=1,\ 2,\ 3,\ \ldots,\ m^J \quad (22b)$$

Again, all local components of physical vectors have been converted to global components by applying Eq. (2).

In previous Eqs. (21a,21b) and (22a,22b), there are $6(m^J+1)$ number of scalar equations, containing $6m^J$ components of dynamic state vectors $\bar{u}_\alpha^s(\bar{u}, \bar{\phi})$ and another $6m^J$ components of $\bar{F}_\alpha^s(\bar{F}, \bar{M})$, ($\alpha$ = 1, 2, …, 6). In addition, among 12 components of joint force $\bar{\mathbf{f}}^J$ and $\bar{\boldsymbol{\mu}}^J$, and joint displacements $\bar{\mathbf{U}}^J$ and $\bar{\boldsymbol{\Phi}}^J$ only 6 can be prescribed according to physical conditions, and the remaining 6 components being extra unknowns. Altogether, we have established from the joint coupling equations $6m^J$ + 6 independent equations for $12m^J$ + 6 unknown dynamic state variables, a shortage of $6m^J$ number of equations.

If all structural members are connected to the common joint by hinges or pins, Eq.(22b) for the local rotations $\bar{\Phi}_K^J$ are replaced by $3m^J$ equations of vanishing moments, $\bar{M}_i^{J\Lambda} = 0$, and Eq. (21b) are trivially satisfied. The new system is still short of $6m^J$ for the equations.

3.2 Scattering Matrices of Joints and Structures

Local Scattering Matrix of A Joint In reverberation ray matrix analysis, we replace the unknown dynamic state variables $\bar{u}_\alpha^s$ and $\bar{F}_\alpha^s$ at the joint ends in previous matrix equations with the unspecified amplitude-coefficients $a_\alpha^{J\Lambda}$ and $d_\alpha^{J\Lambda}$, ($\Lambda = 1\ldots m^J$; α = 1, 2, …, 6) of traveling waves in each member. By substituting the matrix solutions Eqs. (19) and (20) into Eqs. (21a,21b) and (22a,22b), we obtain a large system of algebraic equations for the unknown amplitude coefficients of m^J connecting members, the phase functions at $x^{J\Lambda} = 0$ are reduced to constants of unity. The unknown amplitude coefficients are reassembled to form two large column matrices $\mathbf{a}^J(a_\alpha^{J\Lambda})$ and $\mathbf{d}^J(d_\alpha^{J\Lambda})$ of

https://doi.org/10.1017/jmech.2012.146 Published online by Cambridge University Press

$6m^J$ scalar element each, called joint vector of arriving wave amplitudes, and of departing wave amplitudes at J. In addition, there contained in the same system of equations, the unknown joint displacement $\mathbf{U}^J(U_K^J)$ and $\mathbf{\Phi}^J(\Phi_K^J)$, which can be solved first in terms of displacement components of member $\overline{u}_i^{J\Lambda}$ and $\overline{\phi}_i^{J\Lambda}$ from 6 selected scalar equations of Eqs. (22), the large system of equations for components of $\mathbf{a}^J$ and $\mathbf{d}^J$ is expressed by the following equation,

$$\mathbf{A}^J\mathbf{a}^J + \mathbf{D}^J\mathbf{d}^J + \mathbf{f}^J = 0 \tag{23}$$

In the previous matrix equation, $\mathbf{A}^J$ and $\mathbf{D}^J$ are two sparsely populated square matrices of dimension $6m^J$, consisting geometric and material parameters, wave numbers k_α, and the excitation frequency ω. The column matrix $\mathbf{f}^J$ is composed of 6 components of applied forces and moments $(\overline{f}_K^J)$ and $(\overline{\mu}_K^J)$ at the joint plus $6(m^J - 1)$ null elements of zero.

Pre-multiplying Eq. (23) by $(\mathbf{D}^J)^{-1}(\equiv \mathbf{D}^{-J})$, the inverse of matrix $\mathbf{D}^J$, we obtain

$$\mathbf{d}^J = \mathbf{S}^J\mathbf{a}^J + \mathbf{s}^J \tag{24}$$

where $\mathbf{S}^J = -(\mathbf{D}^J)^{-1}\mathbf{A}^J$, and $\mathbf{s}^J = -(\mathbf{D}^J)^{-1}\mathbf{f}^J$. The $6m^J$ square matrix $\mathbf{S}^J$ is called the *joint-scattering matrix*, and the $6m^J$ column matrix $\mathbf{s}^J$ is called joint (local) source vector.

Physically, the source wave vector $\mathbf{s}^J$ represents waves radiated by the joint-force $\mathbf{f}^J$ and distributed according to the matrix operator $\mathbf{D}^{-J}$ among all connecting members. The joint scattering matrix $\mathbf{S}^J$ which transforms a^J into d^J signifies that incident wave from any member in one of six modes is simultaneously reflected by the joint back to the same member and refracted into all other connecting members, each in six modes. In other words, the joint scattering matrix $\mathbf{S}^J$ transfers an incident ray of arriving wave vector in a member into six reflected rays back to the same member, and $6(m^J-1)$ refracted rays into other connecting members. It is a very complex phenomenon of wave-scattering (reflection, refraction, and transmission) by one joint in a structure.

Scattering Matrices of Loaded Joints If the point mass M^J of each joint is very small in comparison with total mass of adjacent member, the inertia terms in Eqs. (21a,21b) and hence the unknown U_K^J and Φ_K^J are neglected altogether. On the other hand, if M^J are large or U_K^J and Φ_K^J must be computed for added mass, we stack the six components $\mathbf{U}^J$ and $\mathbf{\Phi}^J$ to the end of column matrix $\mathbf{d}^J$ to form extended departing wave joint-vector $\mathbf{d}_1^J$, a column matrix of $6(m^J+1)$ elements. Similarly, we stack six null elements each to the column matrix of $\mathbf{a}^J$ and $\mathbf{f}^J$ to form extended arriving wave joint vector $\mathbf{a}_1^J$ and extended joint force vector $\mathbf{f}_1^J$. The system of $6(m^J+1)$ scalar Eqs. (21ab) and (22ab), including all displacement components are then converted to following matrix equation,

$$\mathbf{D}_1^J\mathbf{d}_1^J + \mathbf{A}_1^J\mathbf{a}_1^J + \mathbf{f}_1^J = 0 \tag{25}$$

In the previous equation, $\mathbf{D}_1^J$ is a $6(m^J+1)$ square matrix, and $\mathbf{A}_1^J$ is a rectangular matrix of $6(m^J+1) \times 6m^J$. Again, by pre-multiplying Eq. (25) with $(\mathbf{D}_1^J)^{-1}$, we obtain another joint scattering matrix similar to Eq. (24) for $\mathbf{D}_1^J$, including joint displacements U_K^J and Φ_K^J.

Global Scattering Matrix of Structure

Continuing the processes of stacking the joint-wave amplitudes $\boldsymbol{d}^J$ and $\boldsymbol{a}^J$ in Eq. (24) for all joints of the structure (J = 1, 2, 3,…, n), we obtain the global departing wave vector $\mathbf{d}(\mathbf{d}^1, \ldots, \mathbf{d}^k, \ldots \mathbf{d}^m)$ and global arriving wave vector $\mathbf{a}(\mathbf{a}^1, \ldots, \mathbf{a}^k, \ldots \mathbf{a}^m)$ of entire structure. Similarly, all joint source-vectors $\mathbf{s}^J(\omega)$ are assembled to form the global source wave vector $\mathbf{s}(\mathbf{s}^1, \ldots, \mathbf{s}^k, \ldots \mathbf{s}^m)$. The three global vectors are then related by the following global scattering matrix formula

$$\mathbf{d} = \mathbf{S}\mathbf{a} + \mathbf{s} \tag{26}$$

where the global scattering matrix $\mathbf{S}$ is composed of n–number of sub-square matrices $\mathbf{S}(\mathbf{S}^1, \ldots, \mathbf{S}^J, \ldots \mathbf{S}^n)$ in square blocks along its main diagonal. The three global vectors $\boldsymbol{d},\boldsymbol{a},\boldsymbol{s}$ in column matrices of previous equation contain a sequence of $12m$ scalar components because each structural member is counted twice in dual coordinate systems in the summing of all joint-amplitude vectors ($\sum_{J=1}^{J=n} n^J = 2m$), and each member-amplitude vector $\mathbf{a}^{J\Lambda}$ or $\mathbf{d}^{J\Lambda}$ has 6 scalar components. Therefore, we have only established $12m$ independent equations in Eq.(26) for $24m$ unknown amplitudes, $12m$ in $\boldsymbol{a}$ and $12m$ in $\boldsymbol{d}$. Another supplementary system of $12m$ equations relating $\boldsymbol{a}$ and $\boldsymbol{d}$ is needed for determining the unknown amplitude coefficients.

3.3 Compatibility Condition for Dual Wave Solutions and Reverberation-Ray Matrix of a Structure

The search for a supplementary system of equations was, however, not straight forward as we have just about exhausted all applicable principles of mechanics and methods of boundary value problems to establish the global scattering Eq. (26). It started with an intuitive observation made by Howard [25] for axial waves in trusses and again by Keh [26] for flexural waves. They observed that the arriving wave at joint J with amplitude a_α^{JK} should differ from the departing wave with amplitude d_α^{KJ} starting at joint K by the phase vector $e^{-ik_\alpha l}$ in the same member. This phase relation was understood to be a consequence of causality condition for the same harmonic wave in dual coordinates [3,19,20] it was found that such a supplementary system of phase relations is necessary for two wave solutions in dual coordinates to be compatible everywhere in the member as discussed in this subsection.

https://doi.org/10.1017/jmech.2012.146 Published online by Cambridge University Press

I. Phase Matrix — According to the sign conventions of physical variables in dual coordinates, Eq. (3), we can express the displacement in the form of vector as

$$\boldsymbol{u}^{JK}(x^{JK}) = (\mp)\boldsymbol{u}^{KJ}(l^{JK} - x^{JK}) \tag{27}$$

where negative sign is for u_x and u_y and plus sign for u_z. Substituting the expressions for the three components in terms of a_α, d_α(α = 1, 2, …, 6) in Eqs. (13), (14), (15) and (16), respectively into Eq. (27), the result of combination gives

$$(a_\alpha^{JK} \pm d_\alpha^{KJ} e^{-ik_\alpha l^{JK}})e^{ik_\alpha x^{JK}} + (a_\alpha^{KJ} e^{ik_\alpha l^{JK}} \pm d_\alpha^{JK})e^{-ik_\alpha x^{JK}} = 0 \tag{28}$$

where the sign of unknown amplitude-coefficients in six modes is positive for α = 5, 6 and plus for α = 1, 2, 3, 4. Introducing the phase matrix $\boldsymbol{P}^{JK}$ to account for the phase shift, we can establish another matrix equation for each member from Eq. (28) as follows

$$\boldsymbol{a}^{JK} = \boldsymbol{P}^{JK}\boldsymbol{d}^{KJ} \tag{29}$$

where $\boldsymbol{P}^{JK}$ is a 6 × 6 diagonal matrix, the elements along the main diagonal being $(-e^{-ik_1 l}, -e^{-ik_2 l}, -e^{-ik_3 l}, -e^{-ik_4 l}, e^{-ik_5 l}, e^{-ik_6 l})^{JK}$.

Next, we assemble $\boldsymbol{a}^{JK}$ in the previous equation for all connecting members to form the joint wave vector $\boldsymbol{a}^J$, and then to the global arriving wave vector $\boldsymbol{a}$ of the structure as mentioned previously. The departing wave vectors from the other end of the member $\boldsymbol{d}^{KJ}$(K = 1, 2, …, m^J) are assembled to form $\tilde{d}^J$, which is a column matrix of $6m^J$ elements, arranged in sequence of $(\boldsymbol{d}^{1J}, \boldsymbol{d}^{2J}, \ldots, \boldsymbol{d}^{KJ}, \ldots, \boldsymbol{d}^{m^J J})^T$, and then into the global vector $\tilde{\mathbf{d}}$. The phase shift equations in the form of Eq. (29) are then assembled to form the following global equation for entire structure,

$$\boldsymbol{a} = \boldsymbol{P}\tilde{\boldsymbol{d}} \tag{30}$$

where $\boldsymbol{P}$ is the global phase matrix containing 12m exponential factors along its main diagonal and zero elements elsewhere. Here, we have designated the global vector for the assemblage of $\boldsymbol{d}^{KJ}$ by $\tilde{\boldsymbol{d}}$ because the components of the joint vector $\boldsymbol{d}^J$ are grouped according to the first index of each member and those in $\tilde{\mathbf{d}}^J$ are grouped according to the second index.

II. Permutation Matrix — Note that the column matrix $\tilde{\boldsymbol{d}}$ in the previous equation and **d** in Eq. (30) contain the same elements but in different permutation, and the sequences of assembling **d** and $\tilde{\mathbf{d}}$ are the same as the sequence of assembling **a**. The sequential orders of the same element in two different column matrices may be related by the following matrix equation,

$$\tilde{\boldsymbol{d}} = \boldsymbol{U}\boldsymbol{d} \tag{31}$$

where the square permutation matrix $\boldsymbol{U}$ (12m × 12m) consists of a single non-vanishing element of unity in each and every row and column. The precise form of $\boldsymbol{U}$ depends on the scheme by which neighboring joints are numbered and the sequence of assembling the $\tilde{\boldsymbol{d}}$ and $\boldsymbol{d}$. From Eqs. (30) and (31), we find that the arriving wave vector and departing wave vector at the same joint of a structure are related by the following equation,

$$\boldsymbol{a} = \boldsymbol{P}\boldsymbol{U}\boldsymbol{d} \tag{32}$$

The previous equation that relates the same $\boldsymbol{a}$ and $\boldsymbol{d}$ as those in Eq. (26) is the required supplementary equation for the determination of all the unknown coefficients.

III. Reverberation-Ray Matrix — Substituting the above equation into Eq. (26), we obtain,

$$\boldsymbol{d} = \boldsymbol{S}\boldsymbol{P}\boldsymbol{U}\boldsymbol{d} + \boldsymbol{s} \tag{33}$$

it reduces further to,

$$\boldsymbol{d} = [\mathbf{I} - \mathbf{R}]^{-1}\boldsymbol{s} \tag{34}$$

where $\boldsymbol{R} = \boldsymbol{S}\boldsymbol{P}\boldsymbol{U}$ is called the *reverberation-ray matrix* of steady-state wave in the structure.

Once the departing wave vector $\boldsymbol{d}$ is determined from the previous equation for a given source wave vector $\boldsymbol{s}$, the unknown arriving wave vector $\boldsymbol{a}$ is either evaluated from $\boldsymbol{a} = \boldsymbol{P}\boldsymbol{U}\boldsymbol{d}$ in Eq. (32) [1,2], or from the following equation,

$$\boldsymbol{a} = \boldsymbol{S}^{-1}(\boldsymbol{d} - \boldsymbol{s}) \tag{35}$$

which is obtained by substituting the solution of $\boldsymbol{d}$ from Eq. (34) into Eq. (26) [3]. Each one of the two expressions for a can be deduced from the other analytically. They yield, however, different approximate result if a truncated Neumann series expansion of the inverse transform $[\mathbf{I}–\mathbf{R}]^{-1}\mathbf{s}$ is used to approximate the value $\boldsymbol{d}$. Details are shown in the next section.

4. DYNAMIC RESPONSES OF A FRAMED STRUCTURE

Once the global wave amplitude vectors **a**(ω) and **d**(ω) are determined from Eqs. (32) and (34) respectively, we can calculate the steady-state response for each member of a structure excited by concentrated forces of harmonic time function, $\bar{f}^J(\omega)\, e^{i\omega t}$ of arbitrary constant frequencies ω at all joints J = 1, 2, …, n from Eqs. (19) and (20). To organize the large amount of numerical work for computing **d**(ω) and **a**(ω) over very large range of ω, we consider first that all joint forces $\mathbf{f}^J(t)$, J = 1, 2, …, n have common scalar time function $f(t)$ with the common Fourier transform $\bar{f}(\omega)$. Joint forces with different time function will be treated successively by superposition.

https://doi.org/10.1017/jmech.2012.146 Published online by Cambridge University Press

The global source wave vector $\mathbf{s}(\omega)$ in Eq. (26) may then be reduced to $\mathbf{s}(\omega) = \bar{f}(\omega)\,\mathbf{s}_\delta(\omega)$. The subscript δ emphasizes that the source wave vector $\mathbf{s}_\delta(\omega)$ is generated by an impulsive joint force with delta time function $\delta(t)$, of which the Fourier transform is a constant unity in frequency domain, $\bar{\delta}(\omega) = 1_\omega$. By this separation, the global wave vectors and $\boldsymbol{d}$ and $\boldsymbol{a}$ are respectively given by

$$\begin{aligned}&\mathbf{d}(\omega) = f(\omega)\mathbf{d}_\delta(\omega) = \bar{f}(\omega)(\mathbf{I}-\mathbf{R})^{-1}\mathbf{s}_\delta(\omega)\,;\\ &\mathbf{a}(\omega) = f(\omega)\mathbf{a}_\delta(\omega) = \bar{f}(\omega)\mathbf{P}_0(\mathbf{k}l)\,\mathbf{U}(\mathbf{I}-\mathbf{R})^{-1}\mathbf{s}_\delta(\omega)\end{aligned} \tag{36}$$

Such a separation allows one to calculate first a large amount of data for the $\mathbf{d}_\delta(\omega)$ and $\mathbf{a}_\delta(\omega)$, independent of the loading time function of the structure.

4.1 Steady-State Response

To evaluate steady-state and transient responses of each and every structural member specified by the matrix Eqs. (19) and (20), we need only six components of $\mathbf{d}^{JK}(\omega)$ and $\mathbf{a}^{JK}(\omega)$, contained in the global wave vectors $\boldsymbol{d}$ and $\boldsymbol{a}$. We thus introduce the extraction matrix $\mathbf{E}^{JK}$, a rectangular matrix of dimension $6 \times 12m$, which serves to extract six elements pertinent to each member from the 12m column matrix $\boldsymbol{a}$ or $\boldsymbol{d}$. The extracting operation is expressed as

$$\begin{aligned}&\mathbf{d}^{JK}\mathbf{E} = \mathbf{E}^{JK}\mathbf{d}\;;\quad \mathbf{d}^{KJ} = \mathbf{E}^{KJ}\mathbf{d}\\ &\mathbf{a}^{JK}\mathbf{E} = \mathbf{E}^{JK}\mathbf{a} = \mathbf{E}^{JK}\left[\mathbf{P}_0(\mathrm{k}l)\mathbf{U}\mathbf{d}\right]\end{aligned} \tag{37}$$

In the rectangular matrix $\mathbf{E}$ of 6 rows and $12m$ columns, there is only one non-zero element of unity in each row; both $\mathbf{E}^{JK}$ and $\mathbf{E}^{KJ}$ pertain to the same number, but in different dual coordinates x^{JK} and x^{KJ}.

Substituting pertinent elements extracted from $\mathbf{d}(\omega)$ and $\mathbf{a}(\omega)$ into Eqs. (19) and (20), we obtain the steady-state response in displacement-state vector $\bar{\mathbf{u}}^s(x,\,\omega)$ as follows

$$\begin{aligned}&\bar{\mathbf{u}}^s(x,\omega) = \mathbf{C}_+^u\mathbf{P}(+\mathbf{k}x)\mathbf{a}^*(\omega) + \mathbf{C}_-^u\mathbf{P}(-\mathbf{k}x)\mathbf{d}^*(\omega) = \bar{f}(\omega)\left\{\bar{\mathbf{u}}_\delta(x,\omega)\right\}\\ &= \bar{f}(\omega)\left\{\mathbf{C}_+^u\mathbf{P}(+\mathbf{k}x)\mathbf{E}^*\left[\mathbf{P}_0(kl)\mathbf{U}\right] + \mathbf{C}_-^u\mathbf{P}(-\mathbf{k}x)\mathbf{E}^*\right\}\left[(\mathbf{I}-\mathbf{R})^{-1}\mathbf{s}_\delta(\omega)\right]\end{aligned} \tag{38}$$

In previous matrix equations, the superscripts JK identifying all physical qualities in the member JK with either coordinate x^{JK} or x^{KJ} are omitted; those in $\mathbf{E}^{JK}$ and $\mathbf{d}^{JK}$ ($\mathbf{a}^{JK}$) are replaced by $\mathbf{E}^*$ and $\mathbf{d}^*(\mathbf{a}^*)$ respectively, where the asterisk indicates either x^{JK} or x^{KJ} coordinate. The state vector $\bar{\mathbf{u}}_\delta(x,\,\omega)$ defined inside the bracelets of last equality, is called system frequency response or impulsive steady state response driven by a unit time harmonic force, $1_\omega e^{i\omega t}$.

Similarly, we obtain the steady-state response of internal force-state vector $\bar{\mathbf{F}}^s(x,\,\omega)$ by changing merely the coefficient matrix $\mathbf{C}_\pm^u$ to $\mathbf{C}_\pm^f$ as follows

$$\begin{aligned}&\bar{\mathbf{F}}^s(x,\omega) = \mathbf{C}_+^f\mathbf{P}(+\mathbf{k}x)\mathbf{a}^*(\omega)\\ &\qquad + \mathbf{C}_-^f\mathbf{P}(-\mathbf{k}x)\mathbf{d}^*(\omega) = \bar{f}(\omega)\left\{\bar{\mathbf{F}}_\delta(x,\,\omega)\right\}\\ &= \bar{f}(\omega)\left\{\mathbf{C}_+^f\mathbf{P}(+\mathbf{k}x)\mathbf{E}^*\left[\mathbf{P}_0(kl)\mathbf{U}\right] + \mathbf{C}_-^f\mathbf{P}(-\mathbf{k}x)\mathbf{E}^*\right\}\\ &\quad\cdot\left[(\mathbf{I}-\mathbf{R})^{-1}\mathbf{s}_\delta(\omega)\right]\end{aligned} \tag{39}$$

Again, the superscripts JK or KJ are omitted. Note that in the Eq. (38) for steady-state response, the inverse of the matrix $[\mathbf{I}–\mathbf{R}]$ is singular when its determinant vanishes

$$\det\left[\mathbf{I}-\mathbf{R}(\omega)\right] = 0 \tag{40}$$

Let $\omega = \omega_k$ ($k = 1, 2, 3, \ldots, \infty$) be the roots of the previous frequency equation, the steady-state response is driven into resonance of very large amplitudes by the applied time harmonic force of frequency $\omega = \omega_k$. The ω_k is called the natural frequency of the structure in free vibration or resonant frequency in forced vibration.

4.2 Transient Responses

The transient response of the structure under the same loading is simply obtained by applying Fourier inverse transform formula in Eq. (4) to steady state responses $\bar{\mathbf{u}}^s$ in Eq. (38) and $\bar{\mathbf{F}}^s$ in Eq. (39). For each structural member, say JK with either x^{JK} or x^{KJ} coordinate, the transient displacement- state vector is given by (superscripts JK and KJ for each member omitted as indicated by the asterisk of $\mathbf{E}^*$)

$$\begin{aligned}&\mathbf{u}^s(x,\,t) = \frac{1}{2\pi}\int_{-\infty}^{\infty}\bar{f}(\omega)\left\{\bar{\mathbf{u}}_\delta^s(x,\,\omega)\right\}e^{i\omega t}d\omega\\ &= \frac{1}{2\pi}\bar{f}(\omega)\left\{\mathbf{C}_+^u\mathbf{P}(+\mathbf{k}x)\mathbf{E}^*\left[\mathbf{P}_0(kl)\mathbf{U}\right] + \mathbf{C}_-^u\mathbf{P}(-\mathbf{k}x)\mathbf{E}^*\right\}\\ &\quad\cdot\left[(\mathbf{I}-\mathbf{R})^{-1}\mathbf{s}_\delta(\omega)\right]e^{i\omega t}d\omega\end{aligned} \tag{41}$$

4.3 The Neumann Expansion and *N*th Order Solutions

In the first work on MRRM by Howard [1], a different procedure to evaluate the inverse Fourier transform was proposed to evaluate the inverse Fourier transform. The procedure begins with the expansion of matrix $(\mathbf{I}–\mathbf{R})^{-1}$ into a power series of $\boldsymbol{R}$, called the Neumann expansion,

$$(\boldsymbol{I}-\boldsymbol{R})^{-1} = \boldsymbol{I} + \boldsymbol{R} + \boldsymbol{R}^2 + \ldots + \boldsymbol{R}^N + \ldots \tag{42}$$

Substituting the power series into Eq. (34), and truncating the series at the terms of Nth power of $\mathbf{R}$ ($N + 1$ terms), we obtain,

$$\mathbf{d}_N(\omega) = (\mathbf{I} + \mathbf{R} + \ldots + \mathbf{R}^N)\,\mathbf{s}_\delta(\omega) \tag{43a}$$

Continuing substitution of $\mathbf{d}_N$ into Eq. (35), in accordance with the correction made in 2003 [3], we find,

$$\mathbf{a}_N(\omega) = \mathbf{S}^{-1}(\mathbf{d}-\mathbf{s}) = \mathbf{P}\mathbf{U}(0 + \mathbf{I} + \mathbf{R} + \ldots + \mathbf{R}^N)\,\mathbf{s}_\delta(\omega) \tag{43b}$$

https://doi.org/10.1017/jmech.2012.146 Published online by Cambridge University Press

The correction is compatible with causality condition for harmonic waves in dual coordinates that the effect $\mathbf{a}^{JK}$ can not proceed the cause $\mathbf{d}^{JK}$. The $\mathbf{d}_N$ and $\mathbf{a}_N$ are called Nth order global departing, and arriving amplitude vectors respectively. The complete expression for Nth order transient displacement-state vector $\mathbf{u}^s_{(N)}(x,\ t)$ for each member (JK) is thus given by (superscripts JK and KJ for each member omitted as indicated by the asterisk of $\mathbf{E}^*$),

$$u^s_{(N)}(x,\ t)=\frac{1}{2\pi}\int_{-\infty}^{\infty}\bar{\mathrm{f}}(\omega)\left\{\mathbf{C}^u_+\mathbf{P}(+\mathbf{k}x)\left[\mathbf{E}^*\mathbf{a}_{(N)}\right]+\mathbf{C}^u_-\mathbf{P}(-\mathbf{k}x)\left[\mathbf{E}^*\mathbf{d}_{(N)}\right]\right\}e^{i\omega t}\mathrm{d}\omega \tag{44}$$

Through the Neumann expansion, the poles of system frequency response in original inverse Fourier transform are thus removed because each term in the power series expansion of $\bar{\mathbf{u}}^s(x,\ \omega)$ is nonsingular along ω axis. Each term of expanded inverse transform can then be integrated numerically with controllable accuracy.

Furthermore, the Neumann series expansion organizes the propagation of wave signals generated by forces at a joint into the rest of a structure in sequential order. The first term of zeroth order $\mathbf{R}^0$ is associated with propagation of the source wave signals into all members as source rays ($\mathbf{d}_0=\mathbf{s}_\delta$). The second term of first order $\mathbf{R}^1$ is associated with waves propagating and scattered (reflected or refracted) once by neighboring joints, and the $N+1$ term of Nth order $\mathbf{R}^N$ is associated with waves being scattered N times by two or more joints along a selected ray path, and so on. By summing transient waves associated with all $(N+1)$ terms, $\mathbf{R}^0+\mathbf{R}^1+\ldots\mathbf{R}^N$, we obtain Nth order transient response in displacement vector as given in Eq. (44).

The zeroth order response $\mathbf{u}^s_{(0)}(x,\ t)$ gives rise to the transient waves emitted by the source joint at time $t=0$, propagating into all connecting members with speed c_0 or c_s for axial and torsional wave, and maximum group velocity c_{gm} for dispersive flexural waves, arriving first at a receiver at $t=t_{(0)}\equiv x/c_{gm}$. The wave-signal continues to advance until the path of length l is interrupted by neighboring joint at $t=l/c_g$. The shortest time interval, $\tau_l=l/c_{gm}-0$ for a signal to cross a member of length l from joint to joint is called transit time for a signal. Hence the zeroth order response is exact solution for entire structure from time $t=0$ to $t=l/c_{gm}$ at which first order scattering takes place. The first order response $\mathbf{u}^s_{(1)}(x,\ t)$ combines effects of source ray (zeroth order), and wave-signals propagating and refracted by a joint into a neighboring member, or reflected back. The first arrival time of first order response $t_{(1)}$ is the sum of transit time τ_l plus τ_x where τ_x is the transit time from the neighboring joints to the receiver. The Nth order solution $\mathbf{u}^s_{(N)}(x,\ t)$ includes all waves that have been scattered once, twice and N times by one to N joints along all possible path connecting the source and receiver. The N times scattered wave signal arrives first at the receiver on one path at time $t=t_{(N)}$, which is the sum of all transit times $\sum\tau_l$ crossing all segments on the path. Wave-signals of slower propagating speeds continue to arrive after $t_{(N)}$, and the Nth order solution remains correct until the first arrival of next order ray at $t=t_{(N+1)}$.

Finally we conclude that various order solutions for transient displacement of state vector $\mathbf{u}^s_{(N)}(x,\ t)$ given in Eq. (44) approximate in ascending order of N the transient response of the structure over entire time span of observation, $0\le t<\infty$. The Nth order transient response $\mathbf{u}^s_{(N)}(x,\ t)$ is, however, exact solution for early time wave motion of the structure, from $t=0$ to $t=t_{(N+1)}$. We thus may ignore wave signals arriving after first arrival of $(N+1)$ order ray and set $\mathbf{u}^s_{(N)}(x,\ t)$ equal to zero for $t>t_{(N+1)}$, so as to minimize wrap around aliasing error of FFT as discussed next.

The afore-mentioned multi-scattered ray paths, transit times, each arrival time t_N of Nth order ray are sorted out and calculated in MRRM and numerical integrations of Fourier integrals in the inverse transform. For axial and torsional wave traveling with constant wave speed $c_1=c_0$ and $c_2=c_s$, the arrival time of each mode of ray is precisely calculated because each corresponding phase factor $e^{-ik_\alpha l}$ in $\mathbf{R}(\omega)$ in steady state solution gives rise to a phase time shift $t-l/c_\alpha$ in transient wave record of Fourier inverse transform. The correspondence may be expressed by a pair formula with operator $\mathcal{F}^{-1}$ in Eq. (4) given $\mathcal{F}^{-1}\left\{\bar{\mathbf{u}}(x,\ \omega)\right\}=\mathbf{u}(x,\ t)$, then,

$$\mathcal{F}^{-1}\left\{e^{-ik_\alpha l}\bar{\mathbf{u}}(x,\ \omega)\right\}=\mathbf{u}(x,\ t-l/c_\alpha)(\alpha=1,\ 2) \tag{45}$$

For flexural wave with phase factor, $e^{-ik_\alpha l}=e^{-\omega(l/c\alpha)}$, $\alpha=3,\ 4,\ 5,\ 6$, where c_α depends on k_α, there is no clear cut phase time shift. In the calculated transient response record, the arrival of a dominant flexural wave signal may be identified from the signal speed c_{gm} of either bending mode or thickness-shear mode, and $c_{gm}\approx c_s$.

4.4 Precise Numerical Evaluation of Early Time Transient Response

To evaluate numerically general transient response of a structure, we perform numerical integration of the inverse Fourier transform of general frequency response $\bar{\mathbf{u}}^s(x,\ \omega)\equiv\bar{\boldsymbol{f}}(\omega)\bar{\mathbf{u}}^s_\delta(x,\ \omega)$ in Eq. (41) to obtain $\mathbf{u}^s(x,\ t)$ as accurately as possible. Alternatively, we set $\bar{\boldsymbol{f}}(\omega)=1_\omega$ to obtain impulsive transient response $\mathbf{u}^s_\delta(x,\ t)$.

Using FFT numerical method, we may have that $\mathbf{u}^s[n]$ is then related to $\mathbf{u}^s(x,\ t)$ as follows:

https://doi.org/10.1017/jmech.2012.146 Published online by Cambridge University Press

$$\mathbf{u}^s[n]-\frac{\pi}{\Omega_0}\mathbf{u}^s(x,\ n\Delta t)=\frac{\pi}{\Omega_0}\sum_{j=-\infty,\,j\neq 0}^{+\infty}\mathbf{u}^s(x,\ n\Delta t+jT_0)\ ,$$
$$n=0,\ 1,\ 2\cdots 2K-1 \tag{46a}$$

where $\mathbf{u}^s(x, n\Delta t)$ is the exact transient response desired, $\mathbf{u}^s[n]$ represents calculated time record of $\mathbf{u}^s(x, t)$ with FFT, $\Omega_0 = \boldsymbol{K}\Delta\omega$, and $T_0 = 2\pi/\Delta\omega$. The summation on the right hand side of Eq. (46 a) is called the wrap-around-aliasing error of applying FFT. The question of how to represent $\pi/\Omega_0\,\mathbf{u}^s(n\Delta t)$ accurately by $\mathbf{u}^s[n]$ is equivalent to how to essentially minimize the absolute value of $\sum_{j=-\infty,\,j\neq 0}^{+\infty}\mathbf{u}^s(x,\ n\Delta t+jT_0)$ and how small the $\Delta\omega$ should be chosen or how large the T_0 should be.

In MRRM, we calculate the Nth order transient time response $\mathbf{u}^s_{(N)}(x, t)$ corresponding to the Nth order Neumann series expansion $(\mathbf{I}+\mathbf{R}+\ldots+\mathbf{R}^N)$, and Eq. (46a) correspondingly becomes

$$\mathbf{u}^s_{(N)}[n]-\frac{\pi}{\Omega_0}\mathbf{u}^s_{(N)}(x,\ n\Delta t)=\frac{\pi}{\Omega_0}\sum_{j=-\infty,\,j=0}^{+\infty}\mathbf{u}^s_{(N)}(x,\ n\Delta t+jT_0) \tag{46b}$$

The aliasing error on the right hand side of Eq. (46b) can be minimized if the T_0 is selected properly. To select the T_0 properly, First, we choose a desired duration of observing transient response $\tau_r = t_f - t_i$, where t_i is the first arrival time of the fastest wave ray, transmitting directly through a minimum number of joints along the shortest path to the receiver; and the t_f is the ending time of observation. Second, we set N in the Neumann series expansion to be an integer larger than the ratio of $t_r / \tau_{\min}$ so as to include signals that are scattered N times at the joints through all possible ray-paths from the source to the receiver, where $\tau_{\min}$ is the minimum time for any one of the three waves to travel through a structural member of length l on the path from the source to a receiver. The T_0 is then selected as $T_0 \geq t_N + \tau_r$. Such a selection enables us to include all arrived signals that have been scattered N times at the joints along the ray-path of propagation. Moreover, because waves arrived after $t = t_{(N+1)}$ do not affect the Nth order transient time response, we may ignore wave signals arriving after first arrival of $(N + 1)$ order ray and set the Nth order transient time response equal to zero for $t > t_{(N+1)}$. The aliasing error on the right hand side of Eq. (46b) is thus minimized , and the transient time response so obtained is thus exact prior to the arrival of the next signal that would be scattered $N + 1$ times.

However, if $\bar{\mathbf{u}}^s_\delta(x, \omega)$ is not treated at all, given the same T_0 as before, then the aliasing error in Eq.(46a) will simply contains all the waves reflected or transmitted by the joins after the time t_N which are of considerable amplitude. Even if the artificial damping is introduced, the numerical result can't be acceptable unless the T_0 is selected to be quite a large one, but the task will be time-consuming.

In order to reduce the aliasing error in FFT further, we need to restrict the applied time function to a finite range. To impose a limit on the applied time function, we may terminate the step time loading ($t \geq t_0$ (= 0)) at the time $t = t_a$, by adding at the source joint an unloading step force $-f_0H(t - t_a)$. This is equivalent to replace the step time loading unlimited in time by a rectangular pulse $f_R(t)$ of finite duration $\tau_a = t_a - t_0$ (= 0), vanishing for $t < 0$ and $t > t_a$. The Fourier transform of the rectangular pulse is $\bar{f}_R(\omega) = f_0(1 - e^{-i\omega t_a})/i\omega$, which equals $f_0\tau_a$ at $\omega = 0$ and oscillates with decaying magnitude as ω increases, and reaches first zeros at $\pm 2\pi/\tau_a$. One half of the frequency interval between two zeros is defined as the bandwidth $\Delta\omega_f^B = 2\pi/\tau_a$ of the rectangular forcing function. The duration of the source time function $f_R(t)$ should be selected slightly larger than desired duration of observing transient response τ_r aforementioned. Incidentally, the value of $K\Delta\omega(= 2\pi K/T_0)$ is usually much larger than $\Delta\omega_f^B(= 2\pi/\tau_a)$, so we select the larger one as the finite range of frequency, say $\Omega_0 = 2\pi K/T_0$.

4.5 Comparison with Traditional Matrix Analysis of Structural Dynamics and New Features of MRRM

As shown in sections 2 and 3, the-MRRM differs from traditional matrix analysis of structural dynamics only in the use of dual coordinates x^{JK} and x^{KJ} (for the same structural member JK), and in the expression of traveling wave solutions Eq. (19) instead of standing waves. These two seemingly minor differences, however, have initiated a new mathematical analysis of wave equations and mechanics of solid and structures. Simply speaking, the MRRM has converted a two-point boundary value problem in single–coordinate for each member or wave guide into two one-point boundary value problems in dual coordinates for the same member. As mentioned at the end of Introduction, details of the differences and comparisons with traditional methods have been discussed in two recent references [20,21]. Following the presentation of matrix equations in previous sections, we summarize again key differences and a few new features here.

(1) Simplications in Treating Boundary Conditions

The use of traveling wave solutions in dual coordinates has greatly simplified the treatment of boundary conditions without applying the method transfer matrix. This is evidenced by the setting up joint coupling Eqs. (22) and (23) at the origin $x = 0$ of each coordinates for determining the unknown amplitude-coefficients $\mathbf{a}^J$ and $\mathbf{d}^J$ of the solution. Because of *the phase factors* are dropped out at one end joint ($x = 0$) in Eq. (23), and components of $\mathbf{a}^J$ and $\mathbf{d}^J$ are devoid of transcendental functions such as $e^{ik_\alpha l}$, $\cos k_\alpha l$ or $\sin k_\alpha l$. Although the unknown components of $\mathbf{a}^J$ and $\mathbf{d}^J$ are twice many as those in traditional methods. The additional system of equations needed is deduced simply from the compatibility conditions for dual wave solutions for the same member [3], in Eq. (27).

https://doi.org/10.1017/jmech.2012.146 Published online by Cambridge University Press

(2) Well-conditioned Matrices for Steady State Response and Natural Frequencies

In the MRRM, each element of the reverberation-ray matrix **R = SPU** in Eq. (34), when properly normalized, is equal or less than unity in magnitude, because that of **S** is always less than 1 and that of diagonal matrix **P** is less than unity for all real wave number k_α. For pure imaginary wave numbers of two thickness shear modes k_4 and k_6, we set $k_\alpha = \pm ik'_\alpha$ ($\alpha = 4, 6$) where k'_α is always positive real, and select the proper imaginary branch of dispersion curves in Fig. 2 so that $e^{\pm ik_\alpha l} = e^{-k'_\alpha l}$, an exponentially decaying factor for increasing k'_α. Therefore, the matrices for the steady state response, Eq. (38), and the frequency determinant of **I**–**R** in Eq. (40) are all well-conditioned.

On the other hand, in the traditional analysis of dynamic equations in single coordinate, base upon the transfer matrix, the solutions for amplitude-coefficients corresponding to $\mathbf{a}^J$ and $\mathbf{d}^J$ always contain standing wave functions $\sin k_\alpha l$ and $\cos k_\alpha l$ which are changed to $\sinh k'_\alpha l$ and $\cosh k'_\alpha l$ ($\alpha = 4, 6$) for imaginary wave numbers of two thickness shear modes. Both hyperbolic functions contain exponentially growing factors $e^{+k'_\alpha l}$ ($\alpha = 4, 6$) which cause numerical instability in matrix evaluations. The seriousness of numerical instability due to ill-conditioned matrix has been noted in many publications [14,27], and so on, for natural frequencies of higher modes in flexural motion. The same problem of numerical instability exists in frequency equations (Thomson-Heskell matrix) of seismic waves in layered media [28]. As reviewed by Pao *et al*. in 2007 [19], many special techniques have been proposed to recondition the ill-behaved matrix but they all have limitations in scope of applicability. On the other hand, the first author of this paper and his associates tried to determine natural frequencies of planar trace and found the well-behaved matrix equation det. (**I**–**R** = 0) and were successful to calculate roots of 10th and higher modes [29]. They continued successfully to calculate normal modes from the matrix equation of steady state response, Eq. (38), transient response of the truss by expansion in series of normal modes, by evaluating amplitude racial of the column vectors $\mathbf{d}^J$ and d from Eq. (24) at $s^J = 0$ [30]. They have also successfully extended the MRRM to determine transient response of structures due to moving loads [31]. Details will be reported in near future.

(3) Eliminating Wraparound Error in Calculating Inverse Fourier Transform by FFT

We have shown in Eq. (44) that the Nth order approximation of transient response in displace is also exact early time response prior to the arrival of $(N + 1)$th order ray from force to the receiver. The inverse Fourier integral could be calculated numerically by applying a FFT algorism. The wraparound aliasing error of FFT is minimized in this case because transient waves arriving after $(N + 1)$th ray has little or low effect on earlier response as explaining by Eqs. (46a,46b).

(4) Clear understanding in Physical Interpretation and Applicable to Wave-Guide Networks of other Wave Phenomena

Following the mathematical derivations by MRRM step by step, one can interpret each step of solution in terms of physics or waves including three wave parameters, $\omega = kc$, for all six modes propagating along six rays of wave in each members; scattering and mode conversion at each structural joint, Eq. (24); and reverberation of multi-scattered rays of waves in a structure, Eq. (34); steady state and transient of wave-responses in the structure steady state and transient waves in the structure, Eqs. (38) and (41). In other words, the very complex phenomena of transient motion and vibration of a multi-connected framed structure is not much different from multiple scattering of elastic waves in a three dimensional network of wave-guides. The clear physical interpretation and understanding of mathematical results implies that the newly developed mathematical method of reverberation-ray matrix MRRM can also be applied to investigate propagation and multi-scattering of acoustic waves, optical waves, electromagnetic signals, microwaves, and many other unidirectional waves in a three dimensional network of wave guides.

5. GENERATION OF SOURCE WAVE-RAYS AND BALANCE OF INTERNAL FORCES AT CORNER JOINTS OF A STRUCTURE

To illustrate calculations of steady-state and transient responses of a three-dimensional structure based upon the reverberation-ray matrix formulations, we consider a two-storey framed building shown in Fig. 1(a), subjected to a horizontal impact force at source joint 1. We show first in this section the calculated transient wave record of forces and moments in all members connected to the loaded joint, and the corner joint 7. The structure is composed of 8 columns and 8 beams with 12 joints ($n = 12$, $m = 16$).

In the calculations all qualities with dimension of length are normalized by basic unit of length l_0, those with dimension of time by basic unit of time $t_0 = l_0 / c_0$, those with dimension of force by $F_0 = El_0^2$, those with dimension of moment by $F_0 l_0$, and $c_0 = \sqrt{E/\rho}$ is propagational wave speed of axial wave. The length of 8 vertical columns in the Y-direction are $3l_0$, that of 4 horizontal beams in the X-direction is $5l_0$, and that of 4 horizontal beams along the Z-direction is $4l_0$. All structural members are made of low carbon steel, and Poisson's ratio v is taken to be 0.3 in computation. All eight horizontal beams are formed by assembling two C-channels (AISC MC18 × 58), and the eight vertical columns by two small C-channels (AISC MC15 × 50) [32]. Data for all material parameters and cross sectional dimensions of C-channels can be found in hand-

https://doi.org/10.1017/jmech.2012.146 Published online by Cambridge University Press

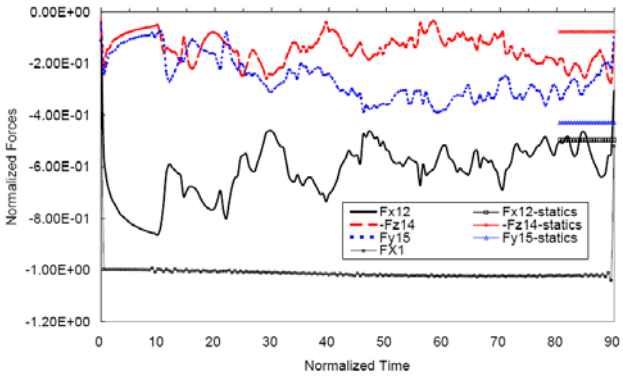
books or standard test of stress material. Numerical data are listed as $A_h = 0.026204 l_0^2$, $\gamma_x / l_0 = 0.1996$, $\gamma_y = 0.4844\gamma_x$ and $\gamma_z = 0.8748\gamma_x$ for horizontal C-channels, and $A_v = 0.022593 l_0^2$, $\gamma_x / l_0 = 0.1682$, $\gamma_y = 0.5026\gamma_x$ and $\gamma_z = 0.8645\gamma_x$ for vertical C-channels. Only one impact force $F_0 H(t)$ is applied at joint 1 along the X-axis. All numerical results for forces and moments shown in this section are calculated first in local coordinates x, y, z, and then converted to components in global coordinates X, Y, Z for purpose of checking the dynamic balance of each joint.

5.1 Balance of Actions and Reactions at Source-Joint

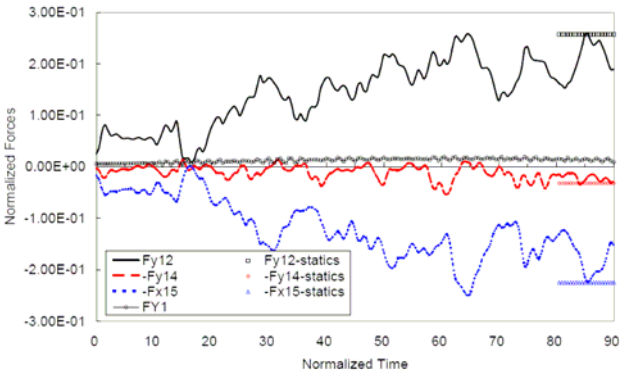
Based upon Eq. (41) with geometrical data and material constants listed previously, we have calculated the transient responses of moments and forces in all structural members connected to the twelve joints of the structure from $t = t_i = 0$ to $t_f = 0.0162(s)$ at $x = 0$ of each local coordinate. The step-time loading function is then terminated with the unloading time-function at $t = T_0 = 0.0596(s)$, from which we set the finite range of frequency $\Omega_0 = 1.7494 \times 10^5 (\text{rad/s})$. The incremental frequency interval of inverse Fourier integral is set at $\Delta\omega = 4.3735(\text{rad/s})$ and the incremental time for the transient response at $\Delta t = 1.7958 \times 10^{-5}(s)$. The highest power of Neumann series expansion (order of approximation) is limited at $N = 30$.

We show first balance of internal forces and moments in three members 1-2, 1-4 and 1-5 at joint 1 with the suddenly applied constant force. Although the wave vectors $\boldsymbol{a} = \boldsymbol{a}(\omega)$ and $\boldsymbol{d} = \boldsymbol{d}(\omega)$ are calculated from balance equations of all forces and moments at each joint in frequency domain, we shall examine if all the forces and moments are also balanced in time domain for the time duration considered. Because the masses of all joints are neglected, the dynamic equilibrium is equivalent to the balance of forces and moments of a joint at all time.

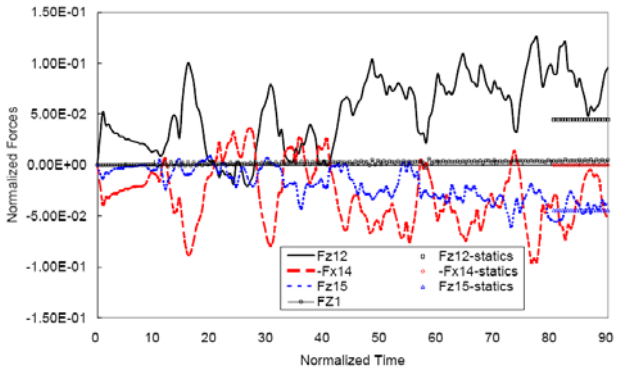
The balance of axial and shear forces at joint 1 in the directions of global X-, Y- and Z-axis is displayed in Fig. 3, whereas the balance of bending and torsional moments is shown in Fig. 4 for the duration 90 normalized time units $(0 \le \bar{t} \le 90)$. It is seen from Fig. 3(a) that the sum of three forces, axial forces F_x^{1-2}, shear forces $-F_z^{1-4}$ and F_y^{1-5} in the X-direction, $F_X^1 = F_x^{1-2} - F_z^{1-4} + F_y^{1-5}$, is of constant value for all time, and equals to the unity in the negative direction, which is balanced precisely by the applied unit step force. The sum of three forces in the Y-direction ($F_Y^1 = F_y^{1-2} - F_y^{1-4} - F_x^{1-5}$) and that in the Z-direction ($F_Z^1 = F_z^{1-2} - F_x^{1-4} + F_z^{1-5}$), are nearly equal to zeros for all time as expected. Similarly, the sum of three moments, torsional moment M_X^1, bending moments M_Y^1, M_Z^1 at joint 1 in three directions, respectively are nearly equal to zeros at all time.



(a) Forces in the global X-direction



(b) Forces in the global Y-direction



(c) Forces in the global Z-direction

Fig. 3 Balance of axial and shear forces in members 1-2, 1-4 and 1-5 at joint 1

5.2 Balance of Forces and Moments at a Free Joint

Next, we consider balance of internal forces and moments at corner joint 7 in the global X-, Y- and Z-directions, respectively as shown in Figs. 5 and 6. The joint 7 is free of external applied force, and its motion is constrained only by four connected members 7-3, 7-6, 7-8 and 7-11. The resultant forces acting at the joint 7 along three global axis, M_X^7, M_Y^7, M_Z^7, and resultant moments M_X^7, M_Y^7, M_Z^7, respectively, are nearly indeed equal to zero for the time interval considered.

In addition to the joint 7, we have calculated internal forces and moments of all members connected to free corner joints 2-6, and 8, the resultant-force and moment acting at the respective joint are indeed nearly equal to zero for all time interval considered. The completeness of the reverberation-ray analysis of steady–state responses of all structure members, and accuracy of

https://doi.org/10.1017/jmech.2012.146 Published online by Cambridge University Press

numerical evaluating inverse Fourier transform with the Neumann series expansion are thus substantiated by the balance of transient wave data for all members shown in Figs. 3 ~ 6.

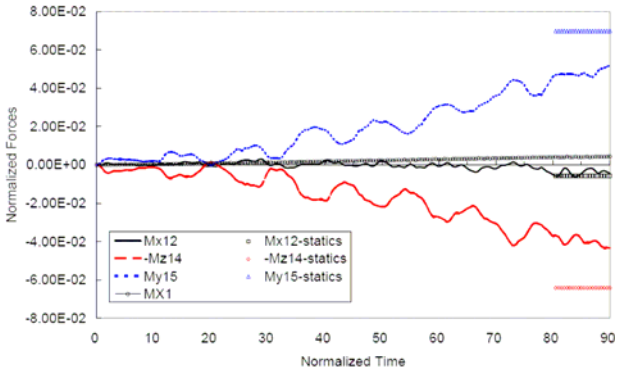
6. GENERATION AND TRANSMISSION WITH MODAL CONVERSION OF TRANSIENT WAVES IN STRUCTURE

The large amount of calculated transient wave records in all structural members connected at the joints shown in Fig. 1(a) furnish a wealth of information for the understanding of dynamic behavior of structures. We have already discussed the balances of forces and moments at loaded and free joints shown in Figs. 3 ~ 6 in the previous section, and shall state additional features response history of other joints we have observed in this section. The seemingly minute and very detailed response history also reveals intricate interplay of physics with mathematics in the reverberation-ray matrix analysis.

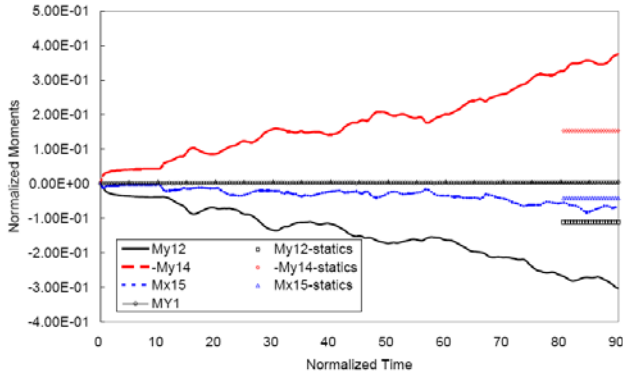
6.1 Generations and Multi-Reflections of Source-Wave-Rays

Impact force applied horizontally at joint 1 generates all six modes of waves, in each of three collecting members 1-2, 1-4 and 1-5, some may be very small in magnitude. Shown in Fig. 7 are time records of the non-dimensional axial force F_x^{12} at joint 1 in member 1-2 for five orders of approximations: i) zero order-source ray in solid line, Is; ii) first order-source ray plus one reflection from all joints in long dash line, $(I + R)s$; iii) second order-source ray plus two reflections from all joints in dot line, $(I + R + R^2)s$; iv) third order- source ray plus three reflections from all joints in dash and dot line, $(I + R + R^2 + R^3)s$; v) fourth order-source ray plus four reflections from all joints in dash and two-dot line, $(I + R + R^2 + R^3 + R^4)s$. The records for all other internal forces and moments are shown in Figs. 3 and 4.

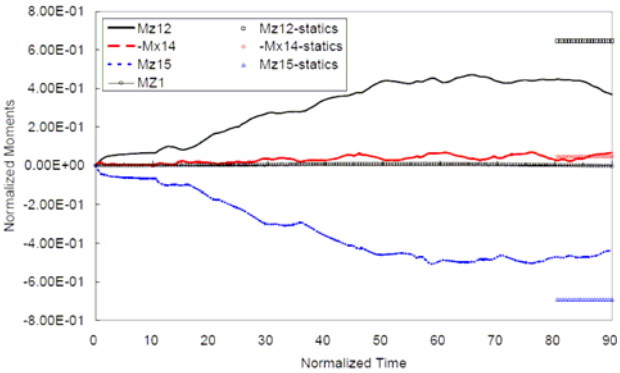
In Fig. 7, the solid line of case i) indicates that the value of the axial force at joint 1 (F_x^{1-2}) in member 1-2 is dropping from 0.0 to –0.5 unit of the force at $\bar{t} = 1.0$, and gradually increases to a constant magnitude of –0.9 or so without any reflection of signals, where $\bar{t} = t/t_0$ is normalized time. Case ii) indicates the effect of one reflection from joint 2 along member 1-2-1 at $\bar{t} = 10$, from joint 4 along the path 1-4-1 at $\bar{t} = 8$ and from joint 5 along the path 1-5-1 at $\bar{t} = 6$. The signals of first reflection from joints 4 and 5 are too small to be seen clearly from the figure. The response curve of case iii) includes twice-reflected waves from all neighboring joints of joint 1. Again, the twice-reflected signals are very small, and the arrival of reflection of joint 2 is marked by a jump at $\bar{t} = 20$. Since the earliest arrival time of twice-reflected wave



(a) Moments in the global *X*-direction



(b) Moments in the global *Y*-direction



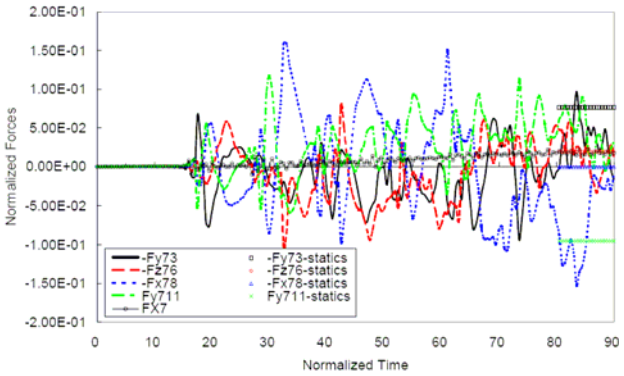
(c) Moments in the global *Z*-direction

Fig. 4 Balance of bending and torsional moments in members 1-2, 1-4 and 1-5 at joint 1

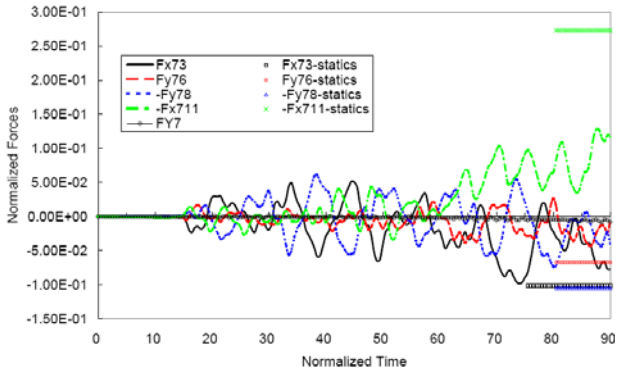
along the shortest path 1-5-1-5-1 is $\bar{t} = 12$, the response curve in case ii) with one ray reflection is the exact value for transmitted waves in member 1-2 up to $\bar{t} = 12$. The twice-reflected signals from joint 5 at $\bar{t} = 12$ and from joint 4 at $\bar{t} = 16$ are noticeable. The response curves of case iv) and v) indicate similar features.

Note that the response curve of case i) (source ray) is significantly different from the well-known step responses of a semi-infinite bar (member 1-2 alone) subject to a step-time impact at one end, the delay in rise time and overshot of magnitude are caused by elastic constraints of members 1-4 and 1-5 at the impact end. In other words, the response in case i) is exact if the

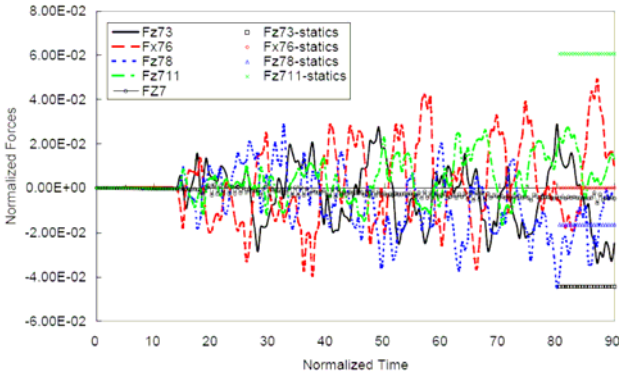
https://doi.org/10.1017/jmech.2012.146 Published online by Cambridge University Press



(a) Forces in the global *X*-direction

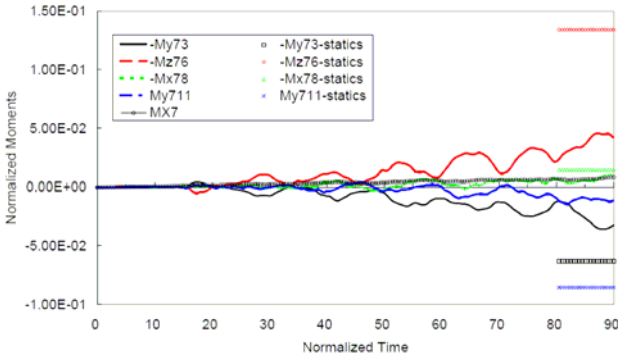


(b) Forces in the global *Y*-direction

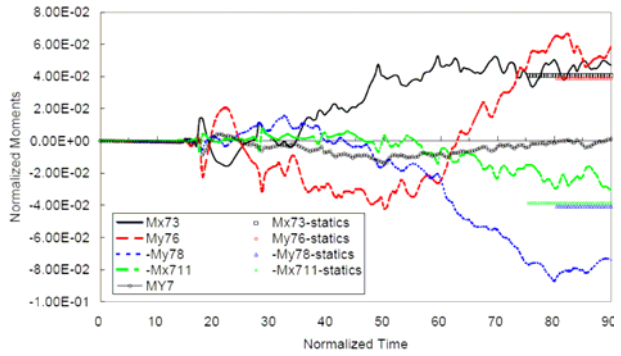


(c) Forces in the global *Z*-direction

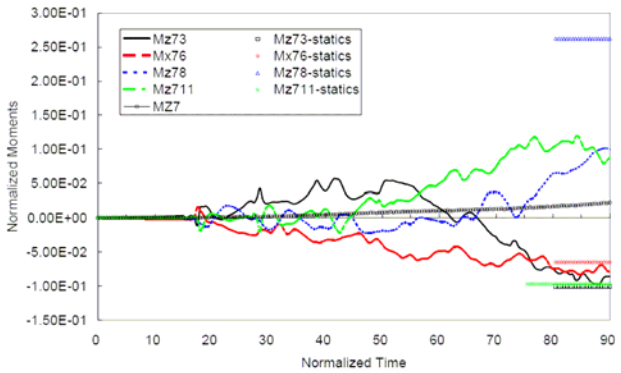
Fig. 5 Balance of axial and shear forces in members 7-3, 7-6, 7-8 and 7-11 at joint 7



(a) Moments in the global *X*-direction



(b) Moments in the global *Y*-direction



(c) Moments in the global *Z*-direction

Fig. 6 Balance of bending and torsional moments in members 7-3, 7-6, 7-8 and 7-11 at joint 7

length of all three connecting members at joint 1 are semi-infinite length. The response case ii) is exact from the framed structure up to $\bar{t} = 10$. One signal reflected from joint 5 arrives and case ii) and iii) are exact up to $\bar{t} = 12$ when twice-reflected signal along the shortest path 1-5-1-5-1 arrives, and so on. These numerical examples exhibit clearly physical significance of Neumann series expansions and various orders of approximation of the solution.

6.2 Arrival Times and Phase Shifts of Three Types of Waves

The accurate arrival time so obtained is, in a way, built in the traveling wave solutions in the matrix Eq. (41). As an example, Fig. 8 displays the forces and

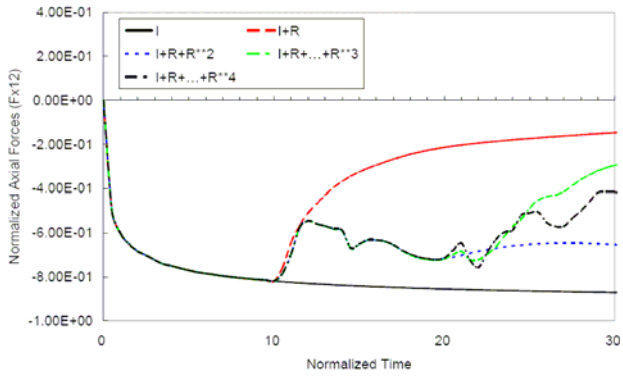
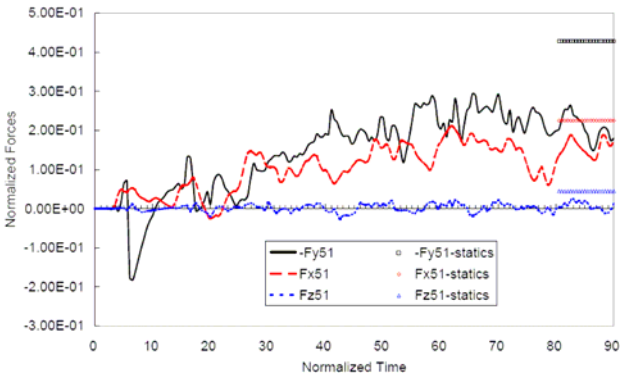


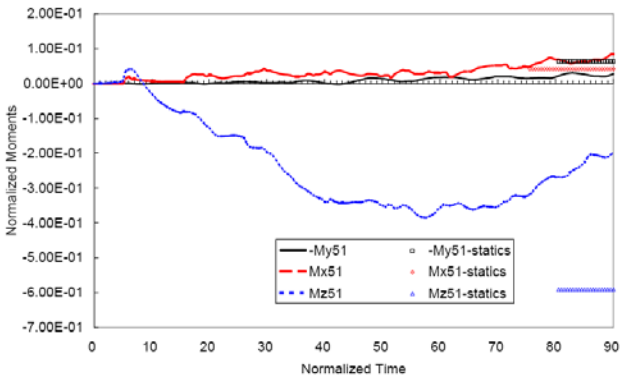
Fig. 7 Transient response of axial force in members 1-2 at joint 1 during early time

https://doi.org/10.1017/jmech.2012.146 Published online by Cambridge University Press

moments at joint 5 in the member 5-1 with length of $3l_0$. The results show that the first arrival times for the axial wave (F_x^{5-1} in Fig. 8(a)) and for the torsional wave (M_x^{5-1} in Fig. 8(b)) are about $\bar{t}=3$ and $\bar{t}=5$, respectively. The first exact arrival time for the latter should be $\bar{t}=3c_0/c_s\approx 4.837$. The arrival time of first arriving signals for the flexural wave in bending mode (M_y^{5-1} and M_z^{5-1} in Fig. 8(b)) is also around $\bar{t}=5$. The calculation indicates that the prediction for the arrival times of signals is very accurate.



(a) Axial and shear forces



(b) Bending and torsional moments

Fig. 8 Forces and Moments in member 5-1 at joint 5

6.3 Transmission with Modal Conversions of Transient Waves from Source to Receiver

When the structure is subjected to a step-time impact at joint 1, all six types of waves are generated in each member connected to this source. Although the torsional moment (M_x^{1-2}, M_x^{1-4}, and M_x^{1-5}) of the source rays generated by the impact force at joint 1 are very small, modal conversion can cause large changes in torsional moments at some other joints. For example, the torsional moment is gradually built up in member 7-3, as shown in Fig. 6(b), through the conversions of source wave (F_x^{1-2} from the source at joint 2, then to large bending moment M_y^{3-2} in member 2-3 at joint 3, through member 2-3 to M_y^{3-2} converting to torsional moment M_x^{3-7}) along six routes, 1-2-3-7, 1-2-6-7, 1-5-6-7, 1-5-8-7, 1-4-3-7, 1-4-8-7. Although the lengths along the ray path are equal, the signal along the first member 1-2 arrives first beams of the shortest traveling time. Dominate effect on torsional moment along 1-2-3-7 at joint 7 is caused by shear force F_z^{2-3} at joint 2 which generates the bending moment M_y^{3-2} at the end of beam 2-3, and coverts to the torsional moment M_x^{3-7} at joint 3. The action is like the rotating about column 3-7. Similar wrench actions are also generated along the other paths.

Conversely, large torsional moment M_x^{7-3} at joint 7 is converted partially to bending moment M_y^{7-8} in member 7-8 and M_y^{7-6} in member 7-6 along the two connected beams. The two bending moments produce a part of torsional moment M_x^{8-12} in column 8-12 and M_x^{6-10} in column 6-10. Through the mode conversion at a joint, the records of transient responses can be used to trace the time history and mode conversions from the source to any receiving location.

In addition, for two columns 5-1 and 7-3, the results indicate that, compared with the maximum value of transient response $M_x^{7-3}=0.0525$ shown in Fig. 6(b), the maximum value of $M_x^{5-1}=0.0846$ shown in Fig. 8(b), has an increase by 61.1%. However, a corresponding increase is only 2.7% for the static case. Hence, it should be noted that a remarkable change in torsional moment probably occurs for dynamic case.

7. CONCLUSIONS

In this paper, we have extended the reverberation-ray analysis of vibration and wave motion in planar structures [1-3] to that of three-dimensional framed structures. In the two-dimensional cases, we consider only two types of wave motion in three modes, the axial motion and the flexural motion (bending and thickness-shear modes) in each structural member, but in three-dimensional cases, we need to consider four types of waves in six modes: Axial, torsional, flexural in one principle plane, and another flexural wave in second principle plane. The doubling of wave modes in each member has not increased much the complexity of matrix analysis as discussed in Sections 3 and 4, but it has increased tremendously the difficulty and amount of numerical work of calculating the transient waves in the structure, shown in Sections 5 and 6.

The computer codes developed to calculate the numerical results shown in these sections has been revised several times since the first version was compiled by the third author for his Ph.D thesis in 1995 [26]. It is only through continuous studies of the theory, and improvement of computational codes (twice before [3] and twice afterwards) that we are able to achieve the precision desired for transient responses. The precise numerical values obtained for the first arrival times for different modes, balances of transient moments and forces at each joint, and asymptotic values for long-time, substantiate also the completeness of matrix analysis of a complicated boundary value problems for elastic wave in a network of structural members inter-

https://doi.org/10.1017/jmech.2012.146 Published online by Cambridge University Press

connected at both end-joints. The computational work has produced a large amount of transient wave data and a wealth of information about dynamics of a structure, such as modal conversion of waves transmitting from joint to joint with precise phase delay time described in section 6. It also reveals intricate interplay of physics with mathematics in the reverberation-ray matrix analysis.

The early time transient responses shown in all figures in this paper are "exact" in a sense that no additional approximation is assumed in the one-dimensional elastodynamic theory. The matrix analysis is rigorous, and the non-singular integrals of Fourier inverse transform can be integrated numerically to any desired precision. So far, we are not able to find in open literature any other numerical result of transient responses in structures of comparable complexity with equal precision. The accurate early time transient responses are essential for estimating dynamic overshot or amplification factor of stress and strains in dynamic structural analysis. They provide also theoretical guide for the designing of ultrasonic and non-destructive inspection or structure health monitoring of a large structure.

ACKNOWLEDGMENTS

This research was supported by two grants from National Science Council, Taiwan, through several grants to National Taiwan University from 1995 to 2003. The second author (GHN) acknowledges gratefully the receiving of an especial grant from National Science Council to visit National Taiwan University in 2001. The authors thank the reviewers for their very constructive comments.

APPENDIX

$$\mathcal{L} = \begin{bmatrix} \frac{d^2}{dx^2} & & & & & & \\ & \frac{d^2}{dx^2} & & & & & \\ & & \frac{d^2}{dx^2} & & -\frac{d}{dx} & & \\ & & \frac{\kappa A c_s^2}{I_z c_0^2}\frac{d}{dx} & \frac{d^2}{dx^2} - \frac{\kappa A c_s^2}{I_z c_0^2} & & & \\ & & & & \frac{d^2}{dx^2} & \frac{d}{dx} & \\ & & & & \frac{\kappa A c_s^2}{I_z c_0^2}\frac{d}{dx} & -\frac{d^2}{dx^2} + \frac{\kappa A c_s^2}{I_z c_0^2} & \end{bmatrix}$$

$$\mathcal{M} = \begin{bmatrix} \frac{1}{c_0^2} & & & & & & \\ & \frac{1}{c_s^2} & & & & & \\ & & \frac{1}{\kappa c_s^2} & & & & \\ & & & \frac{1}{c_0^2} & & & \\ & & & & \frac{1}{\kappa c_s^2} & & \\ & & & & & -\frac{1}{c_0^2} & \end{bmatrix}$$

https://doi.org/10.1017/jmech.2012.146 Published online by Cambridge University Press

$$\mathbf{P}(\pm \mathrm{k}x) = \begin{bmatrix} e^{\pm ik_1 x} & & & & & \\ & e^{\pm ik_2 x} & & & & \\ & & e^{\pm ik_3 x} & & & \\ & & & e^{\pm ik_4 x} & & \\ & & & & e^{\pm ik_5 x} & \\ & & & & & e^{\pm ik_6 x} \end{bmatrix}$$

$$\mathbf{C}_{\pm}^{u} = \begin{bmatrix} 1 & & & & & \\ & 1 & & & & \\ & & 1 & 1 & & \\ & & \pm\alpha_3 & \pm\alpha_4 & & \\ & & & & 1 & 1 \\ & & & & \mp\alpha_5 & \mp\alpha_6 \end{bmatrix}$$

$$\mathbf{C}_{\pm}^{f} = \begin{bmatrix} \pm EAik_1 & & & & & \\ & \pm GI_x ik_2 & & & & \\ & & \pm\kappa AG(ik_3 - \alpha_3) & \pm\kappa AG(ik_4 - \alpha_4) & & \\ & & EI_z\alpha_3 ik_3 & EI_z\alpha_4 ik_4 & & \\ & & & & \pm\kappa AG(ik_5 + \alpha_5) & \pm\kappa AG(ik_6 + \alpha_6) \\ & & & & -EI_z\alpha_5 ik_5 & -EI_z\alpha_6 ik_6 \end{bmatrix}$$

REFERENCES

1. Howard, S. M. and Pao, Y. H., "Analysis and Experiments on Stress Waves in Planar Trusses," *Journal of Engineering Mechanics*, ASCE, **124**, pp. 884–891 (1998).
2. Pao, Y. H., Keh, D. C. and Howard, S. M., "Dynamic Response and Wave Propagation in Plane Trusses and Frames," *AIAA Journal*, **37**, pp. 594–603 (1999).
3. Chen, J. F. and Pao, Y. H., "Effects of Causality and Joint Conditions on Method of Reverberation-Ray Matrix," *AIAA Journal*, **41**, pp. 1138–1142 (2003).
4. Levine, H., *Unidirectional Wave Motions*, North-Holland, Amsterdam (1978).
5. Fellipa, C. A., "A Historical Outline of Matrix Structural Analysis: A Play in Three Acts," *Computers & Structures*, **79**, pp. 1313–1324 (2001).
6. Duncan, W. J. and Collar, A. R., "A Method of the Solution of Oscillations Problems by Matrices," *Philosophical Magazine*, **17**, p. 865 (1934).
7. Duncan W. J. and Collar A. R., "Matrices Applied to the Motions of Damped Systems," *Philosophical Magazine*, **19**, p. 197 (1935).
8. Frazer, R. A., Duncan, W. J. and Collar, A. R., *Elementary Matrices and Some Applications to Dynamics and Differential Equations*, Cambridge University Press, Cambridge (1938).
9. Argyris, J. J. and Kelsey, S., "Energy Theorems and Structural Analysis," *London: Butterworth. (Part I reprinted from Aircraft Engineering*, 26 Oct-Nov, 1954 and 27 April-May, 1955) (1960).
10. Turner, M. J., *The Direct Stiffness Method of Structural Analysis*, Structural and Materials Panel Paper, AGARD Meeting, Aachen, Germany (1959).
11. Myklestad, N. O., "A New Method of Calculating Natural Modes of Uncoupled Bending Vibration," *Journal of the Aeronautical Sciences*, **1**, pp. 153–162 (1944).
12. Thomson, W. T., "Matrix Solution for the Vibration of Non-Uniform Beams," *Journal of Applied Mechanics*, **17**, pp. 337–339 (1950).
13. Thomson, W. T., "Transmission of Elastic Waves Through a Stratified Solid Medium," *Journal Applied Physics*, **21**, pp. 89–93 (1950).
14. Pestel, E. C. and Leckie, F. A., *Matrix Method in Elastomechanics*, McGraw-Hill, New York (1963).
15. Weaver, W. Jr. and Gere, J. M., *Matrix Analysis of Framed Structures*, Van Nonstrand Reinhold, New York (1965).
16. Clough, R. W. and Penzien, J., *Dynamics of Structures*, 3rd Edition, McGraw Hill, New York (1995).
17. Cooley, J. W. and Tukey, J. W., "An Algorithm for the Machine Calculation of Complex Fourier Series," *Mathematics and Computation*, **19**, pp. 297–301 (1965).
18. Doyle, J. F., *Wave Propagation in Structures*, 2nd edition, Springer-Verlag, New York (1997).
19. Pao, Y. H., Chen, W. Q. and Su, X. Y, "The Reverberation-Ray Matrix and Transfer Matrix Analyses of Unidirectional Wave Motion," *Wave Motion*, **44**, pp. 419–438 (2007).
20. Pao, Y. H. and Chen, W. Q., "Elastodynamic Theory of Framed Structures and Reverberation-Ray Matrix Analysis," *Acta Mechanica*, **204**, pp. 61–79 (2009).

https://doi.org/10.1017/jmech.2012.146 Published online by Cambridge University Press

21. Pao, Y. H., Su, X. Y. and Tian, J. Y., "Reverberation Matrix Method for Propagation of Sound in a Multilayered Liquid," *Journal of Sound and Vibration*, **230**, pp. 743–760 (2000).
22. Su, X. Y., Tian, J. Y. and Pao, Y. H., "Application of the Reverberation-Ray Matrix to the Propagation of Elastic Waves in a Layered Solid," *International Journal of Solids and Structures*, **39**, pp. 5447–5463 (2002).
23. Timoshenko, S., *Vibration Problems in Engineering*, 3rd Edition, Van Nostrand Co., New York (1955).
24. Mindlin, R. D., *Introduction to the Mathematical Theory of Vibrations of Elastic Plates*, (Edition By Yang, Jiashi), Baker& Taylor Books (2006).
25. Howard, S. M., "Transient Stress Waves in Trusses and Frames," Ph.D. Dissertation, Department of Theoretical and Applied Mechanics, Cornell University, Ithaca, New York (1990).
26. Keh, D. C., "Analysis of Elastic Wave Propagation and Dynamic Stresses in Three-Dimensional Framed Structures," Ph.D. Dissertation, National Taiwan University, Taiwan (1995).
27. Nagem, R. J. and Williams, J. H., "Dynamic Analysis of Large Space Structure Using Transfer Matrices and Joint Coupling Matrices," *Mechanical Structure and Machine*, **17**, pp. 349–371 (1989).
28. Kennett, B. L. N., *Seismic Wave Propagation in Stratified Media*, Cambridge University Press (1983).
29. Miao, F. X., Sun G. J. and Pao, Y. H., "Vibration Mode Analysis of Frames by the Method of Reverberation Ray Matrix," *Journal of Vibration and Acoustics*, **131**, 051005 (2009).
30. Guo, Y. Q., "Theory of Method of Reverberation Ray Matrix and its Applications," Ph.D. Dissertation, Zhejiang University, China (2008).
31. Jiang, J. Q., "Reverberation Ray Analysis of Inhomogeneous Elastodynamic Equations and Nondestrucrive Inspection of Structures," Ph.D. Dissertation, Zhejiang University, China (2008).
32. Timoshenko, S. and Young, D. H., *Elements of Strength of Materials*, 4th Edition, D. van Nostrand Company, Inc., (1962).

(Manuscript received August 18, 2011,
accepted for publication April 9, 2012.)

https://doi.org/10.1017/jmech.2012.146 Published online by Cambridge University Press